

**Forschungszentrum Karlsruhe**  
Technik und Umwelt

Wissenschaftliche Berichte  
FZKA 5653

# **Analysis of the Electro- dynamics of Subcable Current Distribution in the Superconducting POLO Coil Cable**

**C. Sihler, R. Heller, W. Maurer, A. Ulbricht,  
F. Wüchner**

Institut für Technische Physik  
Projekt Kernfusion

Oktober 1995

---



**Forschungszentrum Karlsruhe**  
**Technik und Umwelt**  
**Wissenschaftliche Berichte**  
**FZKA 5653**

**Analysis of the Electrodynamics of Subcable Current Distribution in  
the Superconducting POLO Coil Cable**

*C. Sihler, R. Heller, W. Maurer, A. Ulbricht, F. Wüchner*

**Institut für Technische Physik**  
**Projekt Kernfusion**

**Forschungszentrum Karlsruhe GmbH, Karlsruhe**  
**1995**

**Als Manuskript gedruckt  
Für diesen Bericht behalten wir uns alle Rechte vor**

**Forschungszentrum Karlsruhe GmbH  
Postfach 3640, 76021 Karlsruhe**

**ISSN 0947-8620**

## ABSTRACT

Unexpected ramp rate limitations (RRL) found in superconducting magnets during the development of magnet systems can be attributed to a current imbalance amongst the cabled strands which leads to a lower than expected quench current. In superconducting magnets the current distribution in the cable during ramping depends mainly on the electromagnetic properties of the system. A detailed analysis of principle causes for RRL phenomena was performed with a model for one half of the POLO coil considering the complete inductance matrix of the cable and the fact that all turns are mutually coupled.

The main results of these calculations are that **unequal contact resistances can not be responsible for RRL phenomena** in coils with parameters comparable to those of the POLO coil and that **already minor geometrical disturbances in the cable structure can lead to major and lasting imbalances in the current distribution of cables with insulated and non-insulated strands.**

During the POLO experiment the half-coil model was employed to get a better understanding of the measured compensated subcable voltages during quench. The good agreement of the calculated and measured results demonstrates the validity of the model for RRL analyses.

## **Untersuchung elektrodynamischer Vorgänge bei der Stromaufteilung im supraleitenden Kabel der POLO-Spule**

### ZUSAMMENFASSUNG

Das Auftreten unerwartet niedriger Grenzwerte für die maximale Stromanstiegsrate, mit der sich ein Magnet ohne Verlust des supraleitenden Zustands ("Quench") erregen läßt, kann auf eine ungleichmäßige Stromaufteilung unter den supraleitenden Strands, aus denen der Leiter aufgebaut ist, zurückgeführt werden. Die Stromverteilung im Leiter eines supraleitenden Magneten hängt hauptsächlich von den elektromagnetischen Eigenschaften des Systems ab. Mit dem Netzwerkmodell einer POLO-Halbspule, das sowohl die vollständige Induktivitätsmatrix des supraleitenden Kabels, als auch die Tatsache, daß alle Windungen magnetisch gekoppelt sind, berücksichtigt, wurde eine detaillierte Untersuchung möglicher Ursachen für eine un-symmetrische Stromaufteilung durchgeführt.

Die wichtigsten Ergebnisse dieser Untersuchung sind, daß **ungleiche Kontaktwiderstände nicht für eine un-symmetrische Stromaufteilung in Magneten**, die ähnliche Parameter wie die POLO-Spule haben, **verantwortlich** gemacht werden können und daß **bereits geringfügige geometrische Unregelmäßigkeiten im Kabelaufbau große und praktisch dauerhafte Strominhomogenitäten im Kabelquerschnitt hervorrufen können. Diese Aussagen gelten sowohl für Kabel mit isolierten Strands, als auch für Kabel, bei denen die Strands nicht elektrisch isoliert sind.**

Während des POLO-Experiments wurde das Halbspulen-Modell dazu verwendet, die in den Sub-Kabeln gemessenen kompensierten Spannungen bei Auftreten eines Quenchs besser zu verstehen. Durch die gute Übereinstimmung der berechneten und bei den Quenchexperimenten gemessenen Ergebnisse wird die Gültigkeit des Modells zur Untersuchung der Ursachen un-symmetrischer Stromaufteilung demonstriert.

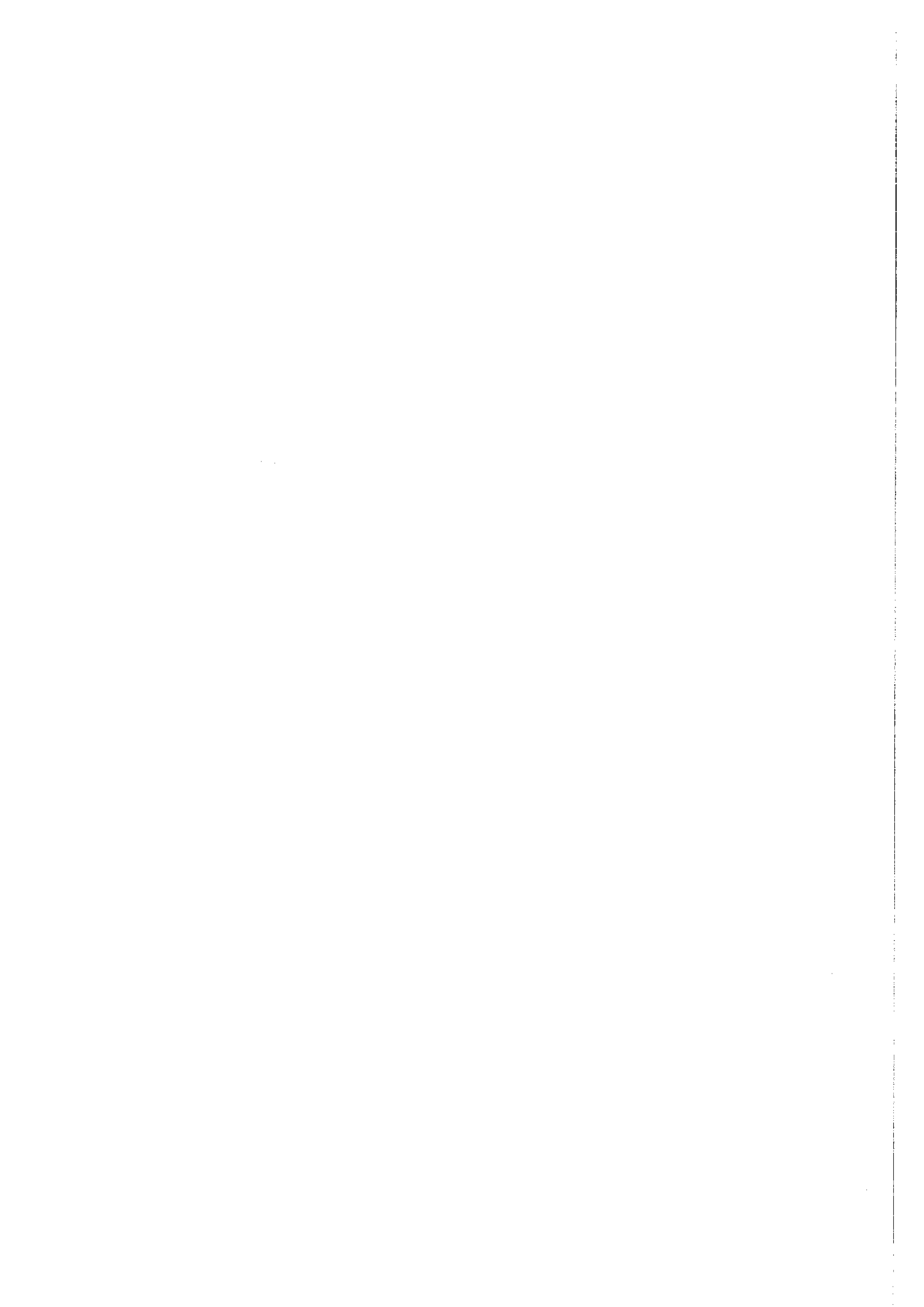


## Table of Contents

<b>I. Introduction</b> .....	5
<b>II. Investigation of subcable current distribution ramping up the superconducting POLO GKG cable</b> .....	7
A. Detailed electromagnetic model of the POLO cable.....	7
B. Analytical investigation of the effects of an unbalanced inductance matrix on the current distribution in the POLO GKG cable.....	10
C. Numerical investigation of the effects of an unbalanced inductance matrix on the current distribution in the POLO GKG cable.....	11
D. Numerical investigation of the effects of unequal contact resistances on the current distribution in the POLO GKG cable.....	13
<b>III. Investigation of subcable current distribution ramping up one half of the superconducting POLO coil</b> .....	15
A. Electromagnetic model for the GKG half of the POLO coil.....	15
B. Numerical investigation of the effects of unequal contact resistances on the current distribution in the GKG cables of the POLO coil.....	16
C. Causes for unbalanced inductance matrices in superconducting magnets.....	18
D. Numerical investigation of the effects of an unbalanced inductance matrix on the current distribution in the GKG cables of the POLO coil.....	21
E. Influence of a transverse conductivity between subcables on the current distribution in the cables of the POLO coil.....	24
<b>IV. Current sharing during quench of the POLO coil - results of calculation and measurement</b> .....	32
A. Quench in the GKG half of the POLO coil.....	32
1. Quench in only one subcable of the GKG half.....	32
2. Quench in all subcables of the GKG half - comparison of calculated and measured results.....	34
B. Quench in the CuNi half of the POLO coil.....	38
<b>V. Conclusion</b> .....	41

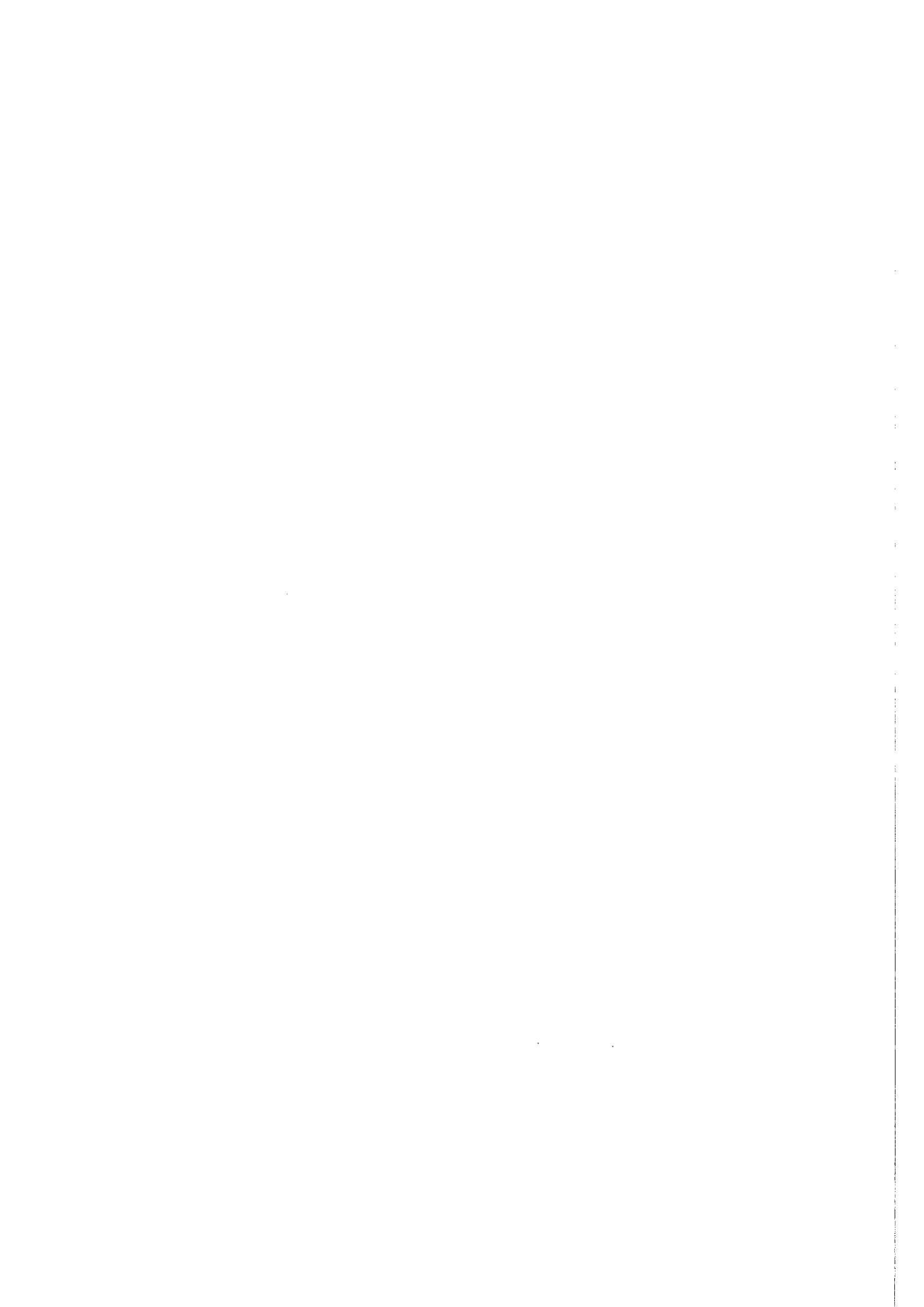


## Table of Figures

Fig. 1. POLO conductor .....	8
Fig. 2. Electromagnetic model of the POLO cable generated with HELIX.....	8
Fig. 3. Equivalent electrical circuit for the POLO GKG cable.....	9
Fig. 4. Current distribution after ramping up the POLO GKG cable to a current of - 20 kA in case of an unbalanced inductance matrix, contact resistances of 3 nΩ, and a cable length of about 10 m.....	12
Fig. 5. Subcable currents after ramping up the POLO GKG cable to a current of - 20 kA in case of an unbalanced inductance matrix, contact resistances of 30 nΩ, and a ten times slower total current rise rate than in Fig. 4.....	12
Fig. 6. Subcable currents after ramping up the POLO GKG cable to a current of - 20 kA in case of unequal contact resistances ( $R_c = 3 \text{ n}\Omega \pm d$ , $d < 1.5 \text{ n}\Omega$ ) and a ramp rate of -1.67 kA/s, cable length about 10 m.....	13
Fig. 7. Subcable currents after ramping up the POLO GKG cable to a current of - 20 kA in case of unequal contact resistances ( $R_c = 30 \text{ n}\Omega \pm d$ , $d < 1.5 \text{ n}\Omega$ ) and a ramp rate of -1.67 kA/s, cable length about 10 m.....	13
Fig. 8. Subcable currents after ramping up the POLO GKG cable to a current of - 20 kA in case of unequal contact resistances ( $R_c = 30 \text{ n}\Omega \pm d$ , $d < 1.5 \text{ n}\Omega$ ) and a ramp rate of -167 A/s, cable length about 10 m.....	14
Fig. 9. Winding cross section of the POLO coil.....	15
Fig. 10. Network model used for the analysis of current distribution in the GKG half of the POLO coil .....	16
Fig. 11. Current distribution in the POLO GKG cable within the first hour (above) and within the first 100 hours (below) after ramping up half of the coil to a current of -20 kA (assumption: contact resistances vary up to 50 %)......	17
Fig. 12. Calculated values of the magnetic coupling factors between adjacent and distant sub-cables.....	18
Fig. 13. Connection between double pancakes .....	20
Fig. 14. Practical embodiment of the connections between double pancakes.....	20
Fig. 15. Current distribution in the POLO GKG cable ramping up half of the coil to a current of -20 kA (assumption: variance of the $M_{i-k}$ values along the winding of 1 ‰ - case 1 of disturbance).....	22
Fig. 16. Current distribution in the POLO GKG cable in the first 100 hours after ramping up half of the coil to a current of -20 kA (assumption: variance of the $M_{i-k}$ values along the winding of 1 ‰ - case 1 of disturbance) .....	22
Fig. 17. Subcable currents in the POLO GKG cable in the first 100 hours after ramping up half of the coil to a current of -20 kA (assumption: variance of the $M_{i-k}$ values within the cable of 1 ‰ - case 2 of disturbance).....	23
Fig. 18. Modification of the model for the GKG half of the POLO coil by introduction of a lumped transverse conductivity at the double pancake connection .....	25

Fig. 20. Currents flowing across the 13 transverse resistances $R_{trans}$ in the POLO half coil model with lumped transverse conductivity after ramping up to a current of -20 kA (same simulation as in Fig. 19) .....	26
Fig. 21. Maximum loss in a single transverse resistance $R_{trans}$ in the POLO half coil model presented in Fig. 18 (same simulation as in Fig. 19) .....	27
Fig. 22. Subcable currents in the POLO half coil model with lumped transverse conductivity after ramping up to a current of -20 kA (assumption: variance of the $M_{i,k}$ values only in the conductors of DP 3, $R_{trans} = 3 \text{ n}\Omega = R_c$ ) .....	29
Fig. 23. Subcable currents in the POLO half coil model with lumped transverse conductivity after ramping up to a current of -20 kA (assumption: variance of the $M_{i,k}$ values only in the conductors of DP 3, $R_{trans} = 30 \text{ n}\Omega = 10R_c$ ) .....	30
Fig. 24. Subcable currents during quench in only one subcable of the POLO GKG conductor (assumption: resistive zone of length $l = 25 \text{ m} = \text{constant}$ in that subcable, corresponding ohmic resistance: $1.1 \text{ m}\Omega$ ) .....	32
Fig. 25. Equivalent POLO cable network for two double pancakes (DP's) with voltage taps for measuring the compensated voltages .....	33
Fig. 26. Calculated compensated voltages of all subcables during quench in only one subcable of the POLO GKG half (assumption: resistive zone of length $l = 25 \text{ m} = \text{constant}$ in that subcable, corresponding ohmic resistance: $1.1 \text{ m}\Omega$ , quench in DP 4) .....	34
Fig. 27. Compensated voltages during quench in DP4 at slowly ramping up to a current of 24.2 kA .....	35
Fig. 28. Measured compensated voltages during quench in DP3 following a half-coil discharge (current level: 27.25 kA in DP3 and DP4, no current in DP1 and DP2) .....	35
Fig. 29. Measured compensated voltages during quench in DP4 at slowly ramping up (coil current: 24.7 kA) .....	36
Fig. 30. Calculated compensated voltages during quench in DP4 (coil current: 25 kA) .....	36
Fig. 31. Calculated subcable currents during quench in DP4 . The currents belong to the compensated voltages in Fig. 30 (same simulation and same time window as in Fig. 30) .....	37
Fig. 32. Calculated subcable currents during quench in DP4 at slowly ramping up. The currents belong to the compensated voltages in Fig. 27 (same simulation and same time window as in Fig. 27) .....	37
Fig. 33. Measured compensated voltage at quench in DP1 and corresponding simulated overall behaviour. ....	38
Fig. 34. Calculated subcable currents belonging to the compensated voltages shown in Fig. 33 .....	39

## I. Introduction

Unexpected periodic variations of the magnetic field were found along the axis of superconducting accelerator magnets which reduces their field quality [1]. The periodic modulation and the size of the field variation can only be explained by a non-uniform current distribution within the cable [2]. They may be caused by extra currents ("supercurrents" [3]) which are induced along the conductor and flow over long cable lengths.

Supercurrents do not only degrade the field quality of accelerator magnets, but also have a strong influence on magnet stability. They may explain the ramp rate limitation (RRL) phenomena observed in magnets developed for fusion [4]. Following tests of the US-DPC in Japan at the end of 1990 [5], small scale tests using a 27 strand Cable-in-Conduit-Conductor (CICC) extracted from the 225 strand US-DPC cable were performed at MIT [6]. All tests identified a profound RRL phenomenon. Recent experiments with a 0.8 m long CICC using local field sensors to study current distribution within the cable registered one or more fast time-scale "disturbances" during field ramps [7]. The observed disturbances seen by the sensor quantitatively correspond to the quenching of a single strand with a current 2-3 times higher than the average strand current. A simple model for the analysis of that phenomenon did not produce a convincing fit to the measured data but showed that current imbalances can be expected to adversely affect the stability of a cable and that the  $\dot{B}$  dependence in the model seems to qualitatively match the observed data [8].

Even though a cable is composed of multiple twisted stages, there is no guarantee that voltages induced by magnetic field changes completely cancel when integrated over the length of the cable. Even in the ideal case of completely transposed strands such voltages still appear due to the unavoidable space dependence of  $\dot{B}$  [9]. Local magnetic field sweep rates of 240 T/s were achieved with the POLO coil without quench [10]. Therefore, it may be assumed that the space dependence of  $\dot{B}$  within a twist pitch can not be responsible for large supercurrents, if the twist pitch length of the cables used in superconducting magnets developed for fusion is comparable to the twist pitch length of the POLO cable (subcable twist pitch length = 40 mm, twist pitch length of round cable with GKG subcables = 229 mm, twist pitch length of round cable with CuNi subcables = 256 mm) [11].

Inductive voltages between subcables can also be caused by disturbances in the symmetrical structure of the conductor which may result from cabling. Compared with the POLO cable other cable types are more critical to such disturbances. Producing long lengths of other cable types minor variances in the electromagnetic properties along the cable can not be excluded for technical reasons. This will be explained in chapter III in more detail.

In a magnet even small inductive voltages can cause large loop currents due to the relatively low resistance between strands in the typically highly compacted, solder-filled joints. Added to the overall transport current, these loop currents dictate the current distribution amongst the strands of the cable [8]. The time constants involved with these loop currents can not be estimated by simplified cable models. Time constants of more than 100 h were measured in some cases [12]. That makes it worth analysing whether the causes for loop currents in short-length cables [13] can be transferred to the problems of superconducting magnets. Such an analysis can only be performed with a detailed electrodynamic model of the magnet considering the inductive coupling of all subcables and the mutual couplings between the turns of the magnet.

Such a model was developed for the POLO coil in order to investigate the electrodynamic behaviour of the cable during quench. The fact that a purely electromagnetic cable model can lead to accurate calculation results for the current sharing process was observed earlier testing an insulated 7-strand cable [14]. It was observed that the quench behaviour of superconducting parallel circuits does not depend so much on the thermal properties of the system, but it rather depends on its electromagnetic properties. The validity of the electromagnetic coil model is confirmed by the good agreement of the calculated and measured compensated sub-cable voltages during quench [10]. More of these results will be presented in the last section of this report. Since the analysis of current sharing in non-insulated strands is very complicated even for simplified cable models [9, 15 -16] or cables of short lengths [14, 17], the analysis of current redistribution after quench in a real-size magnet was concentrated on that half of the POLO coil where the subcables are insulated from each other by Glass-Kapton-Glass (GKG) strips [11].

The first sections of this report deal with the derivation of the electromagnetic coil model and a detailed analysis of causes for RRL phenomena in coils being wound from cables with insulated strands. In the subsequent section a transverse conductance is introduced at the conductor joints. This modification leads to some important results which may be transferred to RRL phenomena in coils being wound from cables with non-insulated strands.

## II. Investigation of subcable current distribution ramping up the superconducting POLO GKG cable

This chapter deals with the electrodynamics of a single turn (cable length  $\approx 10$  m) extracted from the POLO winding. The electrodynamics of subcable current distribution in a superconducting winding with many turns being all mutually coupled is investigated in chapter III - IV.

### A. Detailed electromagnetic model of the POLO cable

In order to be able to calculate the inductance matrix of the POLO conductor which is shown in Fig. 1, a model suited for a numerical calculation with EFFI [18] had to be developed. EFFI allows the calculation of electromagnetic fields, forces, and inductances of coreless magnetic systems. Since even modestly complex coils give rise to very long EFFI input files and in order to ease life for the family of helical coils, the HELIX input generator was developed [19]. Using that input generator one complete turn of the POLO coil could be modelled considering all 13 helically wound subcables of the POLO cable. Part of that model is shown in Fig. 2.

Since computations with a model for the whole cable would have taken days on an IBM 3090 mainframe, only the following magnetic properties of one turn with average length were calculated numerically:

Subcable self inductance:	$L_{1-1} = 12.32 \mu\text{H}$
Subcable mutual inductances:	$M_{1-2} = 10.18 \mu\text{H} = M_{1-13}$
	$M_{1-3} = 8.924 \mu\text{H} = M_{1-12}$
	$M_{1-4} = 8.267 \mu\text{H} = M_{1-11}$
	$M_{1-5} = 7.867 \mu\text{H} = M_{1-10}$
	$M_{1-6} = 7.594 \mu\text{H} = M_{1-9}$
	$M_{1-7} = 7.499 \mu\text{H} = M_{1-8}$

The inductance matrix  $\underline{\mathbf{M}}$  of one turn of the POLO cable can be generated from these data. The fact that the subcables were modelled as conductors with rectangular instead of round cross-section hardly influences the accuracy of the numerically calculated values: The self-inductance of one turn of the POLO coil which results from that matrix is  $8.7 \mu\text{H}$ . That value corresponds well to earlier calculated values for the self-inductance of one turn. Assuming that a turn consists of a solid wire of about the same diameter [20] as the calipered diameter of the stranded combination leads to a self-inductance value of  $9.5 \mu\text{H}$  [21]. Since the here performed investigations are focused on the subcable current **distribution**, the accuracy of this cable model seems to be sufficient.

One half of the POLO coil (winding length 300 m) has a conductor where the subcables are wrapped by CuNi tape. In the other half the subcables are electrically insulated from each other by GKG strips. Knowing the cable inductance matrix  $\underline{\mathbf{M}}$  of one turn, an equivalent electrical circuit for one turn of the GKG half of the POLO coil can be derived as illustrated in Fig. 3. In that figure it is assumed that the subcables are electrically contacted at the beginning and at the end of the turn by ohmic resistances  $R_c$ .

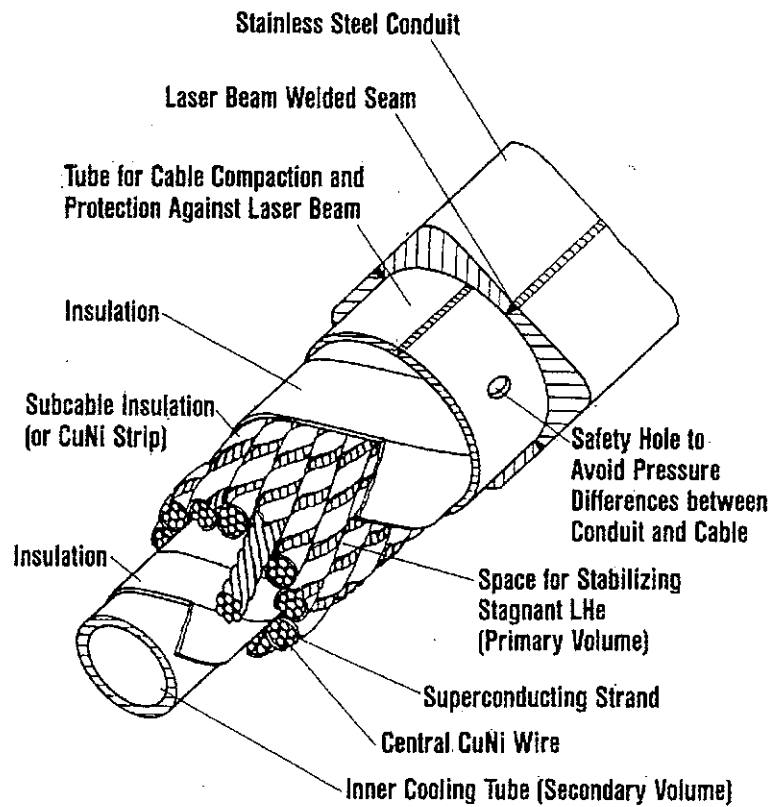


Fig. 1. POLO conductor [11]

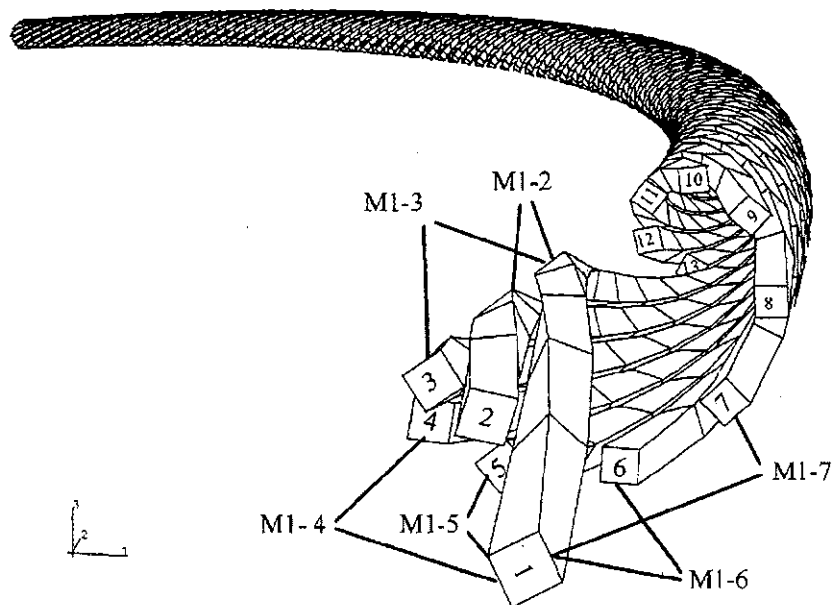


Fig. 2. Electromagnetic model of the POLO cable generated with HELIX [19]

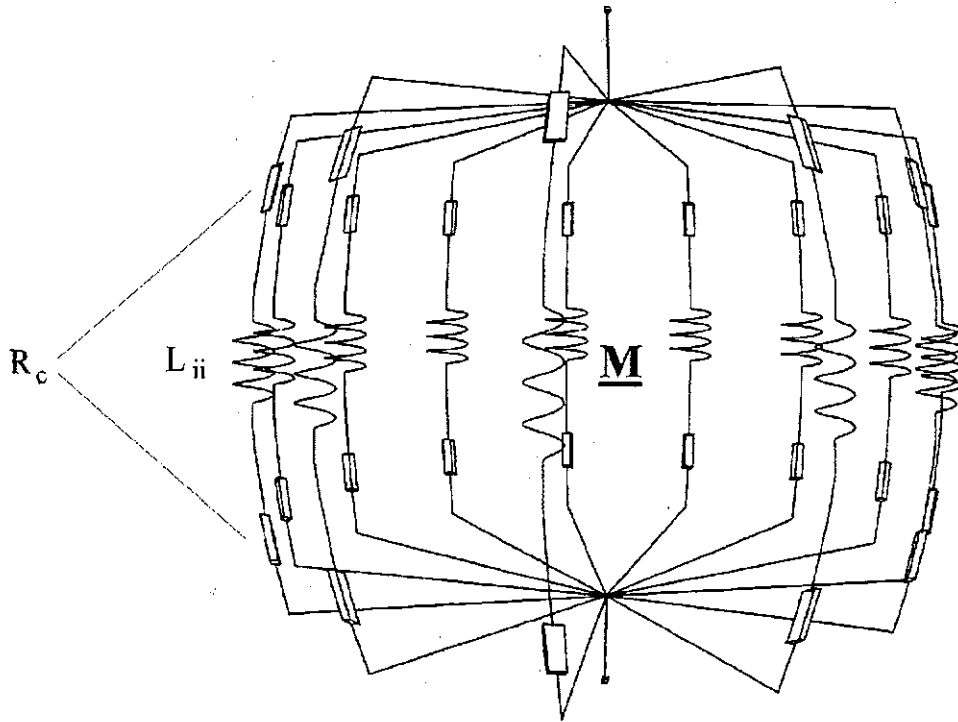


Fig. 3. Equivalent electrical circuit for the POLO GKG cable

The subcable currents in this electrical network can be calculated from the linear differential equation system (1):

$$\underline{\mathbf{M}} \cdot \dot{\mathbf{i}} + 2R_c \cdot \mathbf{i} = \underline{\mathbf{u}}_q(t) \quad ; \quad \underline{\mathbf{u}}_q(t): \text{vector of externally applied voltage}$$

$$\dot{\mathbf{i}} = \frac{d\mathbf{i}}{dt}$$

⇔

$$\begin{pmatrix} L_{1-1} & M_{1-2} & M_{1-3} & M_{1-4} & M_{1-5} & M_{1-6} & M_{1-7} & \dots & M_{1-13} \\ & L_{2-2} & M_{2-3} & M_{2-4} & M_{2-5} & M_{2-6} & M_{2-7} & \dots & M_{2-13} \\ & & L_{3-3} & M_{3-4} & M_{3-5} & M_{3-6} & M_{3-7} & \dots & M_{3-13} \\ & & & L_{4-4} & M_{4-5} & M_{4-6} & M_{4-7} & \dots & M_{4-13} \\ & & & & L_{5-5} & M_{5-6} & M_{5-7} & \dots & M_{5-13} \\ & & & & & L_{6-6} & M_{6-7} & \dots & M_{6-13} \\ & & & & & & L_{7-7} & \dots & M_{7-13} \\ & & & & & & & \ddots & \vdots \\ & & & & & & & & L_{13-13} \end{pmatrix} \begin{pmatrix} i_1(t) \\ i_2(t) \\ i_3(t) \\ i_4(t) \\ i_5(t) \\ i_6(t) \\ i_7(t) \\ \vdots \\ i_{13}(t) \end{pmatrix} + 2R_c \cdot \begin{pmatrix} i_1(t) \\ i_2(t) \\ i_3(t) \\ i_4(t) \\ i_5(t) \\ i_6(t) \\ i_7(t) \\ \vdots \\ i_{13}(t) \end{pmatrix} = \begin{pmatrix} u_q(t) \\ \vdots \\ u_q(t) \end{pmatrix} \quad (1)$$

sym

## B. Analytical investigation of the effects of an unbalanced inductance matrix on the current distribution in the POLO GKG cable

Assuming that

- the contact resistances  $R_c$  are negligible compared to the reactances,
- all initial currents are zero, and
- the applied voltage is a constant voltage  $U_0$ ,

the current rise functions  $\dot{i}_i(t)$  can be calculated directly from the linear equation system (2):

$$\begin{pmatrix} L_{1-1} & M_{1-2} & M_{1-3} & M_{1-4} & M_{1-5} & M_{1-6} & M_{1-7} & \dots & M_{1-13} \\ & L_{2-2} & M_{2-3} & M_{2-4} & M_{2-5} & M_{2-6} & M_{2-7} & \dots & M_{2-13} \\ & & L_{3-3} & M_{3-4} & M_{3-5} & M_{3-6} & M_{3-7} & \dots & M_{3-13} \\ & & & L_{4-4} & M_{4-5} & M_{4-6} & M_{4-7} & \dots & M_{4-13} \\ & & & & L_{5-5} & M_{5-6} & M_{5-7} & \dots & M_{5-13} \\ & & & & & L_{6-6} & M_{6-7} & \dots & M_{6-13} \\ & & & & & & L_{7-7} & \dots & M_{7-13} \\ & & & & & & & \ddots & \vdots \\ & & & & & & & & L_{13-13} \end{pmatrix} \begin{pmatrix} \dot{i}_1(t) \\ \dot{i}_2(t) \\ \dot{i}_3(t) \\ \dot{i}_4(t) \\ \dot{i}_5(t) \\ \dot{i}_6(t) \\ \dot{i}_7(t) \\ \vdots \\ \dot{i}_{13}(t) \end{pmatrix} = \begin{pmatrix} u_0 \\ \vdots \\ u_0 \end{pmatrix} \quad (2)$$

As long as the cable structure is exactly symmetrical, it is evident that the current rise functions in (3) are the solution of this equation system.

$$\dot{i}_1(t) = \dot{i}_2(t) = \dot{i}_3(t) = \dot{i}_4(t) = \dot{i}_5(t) = \dot{i}_6(t) = \dot{i}_7(t) = \dot{i}_8(t) = \dot{i}_9(t) = \dot{i}_{10}(t) = \dot{i}_{11}(t) = \dot{i}_{12}(t) = \dot{i}_{13}(t) = \text{const.} \quad (3)$$

Only a slight change in the symmetrical structure of the inductance matrix can lead to quite a different result. That can easily be demonstrated assuming a case where the mutual inductances between subcable 7 and all other subcables are one percent lower than indicated above for subcable 1. The values of the self inductances and of all other mutual inductances are assumed to stay the same.

Seen from a practical point it is hardly possible to change the symmetrical structure of a cable in such a way that the mutual inductances involved with one subcable get changed by exactly the same percentage. It must be considered that, e.g.,  $M_{1-2}$  and  $M_{1-3}$  differ by 14 %, whereas  $M_{1-6}$  and  $M_{1-7}$  differ by only 1.3 %, so that the considered case of changing all mutual couplings involved with one subcable by 1 % is not of any practical relevance. That case is a purely mathematical example allowing to demonstrate the nontrivial effects of an unbalanced magnetic coupling matrix. Cases of unbalanced coupling matrices which have practical relevance will be investigated in the following sections of this report.

Since the decrease of the mutual inductances  $M_{7-i}$  and  $M_{i-7}$  ( $i=1\dots 13$ ,  $i \neq 7$ ) by one percent is the only disturbance of the symmetrical structure of the inductance matrix, the solution in that case must obey the conditions

$$\dot{i}_6(t) = \dot{i}_8(t), \quad \dot{i}_5(t) = \dot{i}_9(t), \quad \dot{i}_4(t) = \dot{i}_{10}(t), \quad \dot{i}_3(t) = \dot{i}_{11}(t), \quad \dot{i}_2(t) = \dot{i}_{12}(t), \quad \text{and } \dot{i}_1(t) = \dot{i}_{13}(t) \quad (4).$$

Considering these equations in (2) leads to the following equation system for  $\dot{i}_1(t), \dot{i}_2(t), \dots, \dot{i}_7(t)$ :

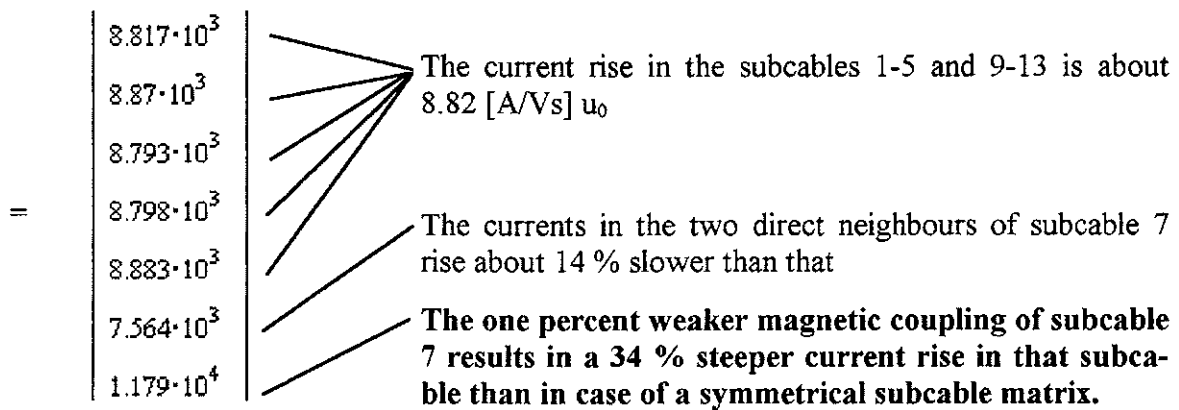
$$\begin{pmatrix} L_{1-1}+M_{1-13} & M_{1-2}+M_{1-12} & M_{1-3}+M_{1-11} & M_{1-4}+M_{1-10} & M_{1-5}+M_{1-9} & M_{1-6}+M_{1-8} & M_{1-7} \\ M_{2-1}+M_{2-13} & L_{2-2}+M_{2-12} & M_{2-3}+M_{2-11} & M_{2-4}+M_{2-10} & M_{2-5}+M_{2-9} & M_{2-6}+M_{2-8} & M_{2-7} \\ M_{3-1}+M_{3-13} & M_{3-2}+M_{3-12} & L_{3-3}+M_{3-11} & M_{3-4}+M_{3-10} & M_{3-5}+M_{3-9} & M_{3-6}+M_{3-8} & M_{3-7} \\ M_{4-1}+M_{4-13} & M_{4-2}+M_{4-12} & M_{4-3}+M_{4-11} & L_{4-4}+M_{4-10} & M_{4-5}+M_{4-9} & M_{4-6}+M_{4-8} & M_{4-7} \\ M_{5-1}+M_{5-13} & M_{5-2}+M_{5-12} & M_{5-3}+M_{5-11} & M_{5-4}+M_{5-10} & L_{5-5}+M_{5-9} & M_{5-6}+M_{5-8} & M_{5-7} \\ M_{6-1}+M_{6-13} & M_{6-2}+M_{6-12} & M_{6-3}+M_{6-11} & M_{6-4}+M_{6-10} & M_{6-5}+M_{6-9} & L_{6-6}+M_{6-8} & M_{6-7} \\ M_{7-1}+M_{7-13} & M_{7-2}+M_{7-12} & M_{7-3}+M_{7-11} & M_{7-4}+M_{7-10} & M_{7-5}+M_{7-9} & M_{7-6}+M_{7-8} & L_{7-7} \end{pmatrix} \begin{pmatrix} i_1^{(0)} \\ i_2^{(0)} \\ i_3^{(0)} \\ i_4^{(0)} \\ i_5^{(0)} \\ i_6^{(0)} \\ i_7^{(0)} \end{pmatrix} = \begin{pmatrix} u_0 \\ u_0 \\ u_0 \\ u_0 \\ u_0 \\ u_0 \\ u_0 \end{pmatrix}$$

$$\Leftrightarrow \underline{\mathbf{M}}_S \cdot \underline{\mathbf{i}} = \underline{\mathbf{u}}_0$$

The current rise functions are directly proportional to the product of  $\underline{\mathbf{M}}_S^{-1} \cdot \underline{\mathbf{e}}$ , where  $\underline{\mathbf{e}}$ : unit vector.

$$\underline{\mathbf{M}}_S^{-1} \cdot \underline{\mathbf{e}} / [A/Vs] =$$

$$\begin{bmatrix} 12.32 + 10.18 & 10.18 + 8.924 & 8.924 + 8.267 & 8.267 + 7.867 & 7.867 + 7.594 & 7.594 + 7.499 & 7.424 \\ 10.18 + 8.924 & 12.32 + 8.267 & 10.18 + 7.867 & 8.924 + 7.594 & 8.267 + 7.499 & 7.867 + 7.499 & 7.518 \\ 8.924 + 8.267 & 10.18 + 7.867 & 12.32 + 7.594 & 10.18 + 7.499 & 8.924 + 7.499 & 8.267 + 7.594 & 7.788 \\ 8.267 + 7.867 & 8.924 + 7.594 & 10.18 + 7.499 & 12.32 + 7.499 & 10.18 + 7.594 & 8.924 + 7.867 & 8.184 \\ 7.867 + 7.594 & 8.267 + 7.499 & 8.924 + 7.499 & 10.18 + 7.594 & 12.32 + 7.867 & 10.18 + 8.267 & 8.835 \\ 7.594 + 7.499 & 7.867 + 7.499 & 8.267 + 7.594 & 8.924 + 7.867 & 10.18 + 8.267 & 12.32 + 8.924 & 10.08 \\ 7.424 + 7.424 & 7.518 + 7.518 & 7.788 + 7.788 & 8.184 + 8.184 & 8.835 + 8.835 & 10.08 + 10.08 & 12.32 \end{bmatrix}^{-1} \begin{bmatrix} 1 \\ 1 \\ 1 \\ 1 \\ 1 \\ 1 \\ 1 \end{bmatrix} =$$



Although only 24 mutual inductances of the cable inductance matrix were decreased by 1 %, the highest increase in current rise is 34 %. The physical reason for the overproportional current rise rate in subcable 7 are the underproportional current rise rates in subcables 6 and 8 which can be explained by Lenz's Law.

### C. Numerical investigation of the effects of an unbalanced inductance matrix on the current distribution in the POLO GKG cable

Simulating the transient reaction of the electromagnetic cable network shown in Fig. 3 with a circuit analysis program [22] leads to almost the same results as in the analytical example if contact resistances  $R_c = 3 \text{ n}\Omega$  are used (Fig. 4), instead of neglecting  $R_c$  as in section II.B.

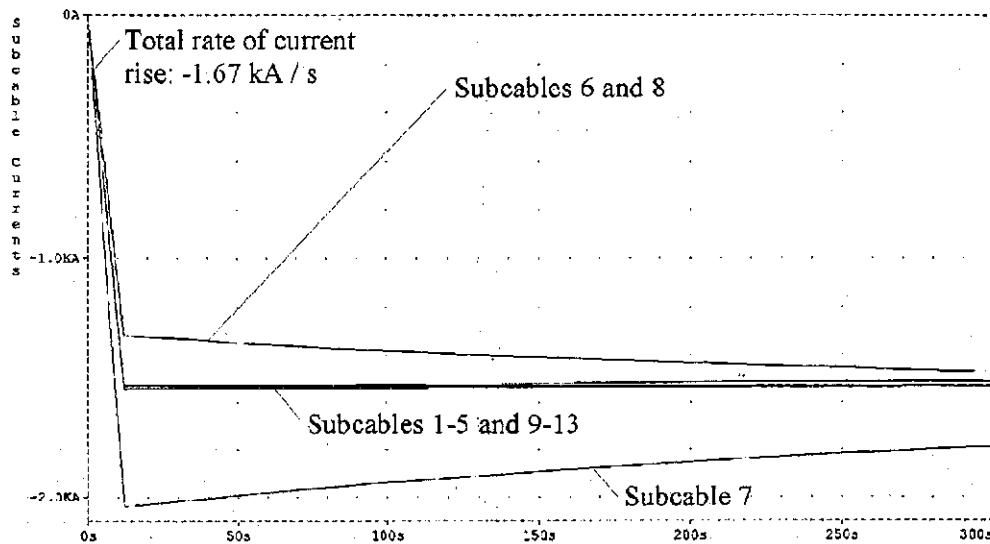


Fig. 4. Current distribution after ramping up the POLO GKG cable to a current of - 20 kA in case of an unbalanced inductance matrix, contact resistances of  $3 \text{ n}\Omega$ , and a cable length of about 10 m

The shorter the cable length is, the higher the contact resistances are and the slower the total current rise rate is, the less visible is the effect of unbalanced cable matrices. Assuming the same cable length as in Fig. 4 the quantitative effects of higher contact resistances and a slower total current rise rate is demonstrated in Fig. 5.

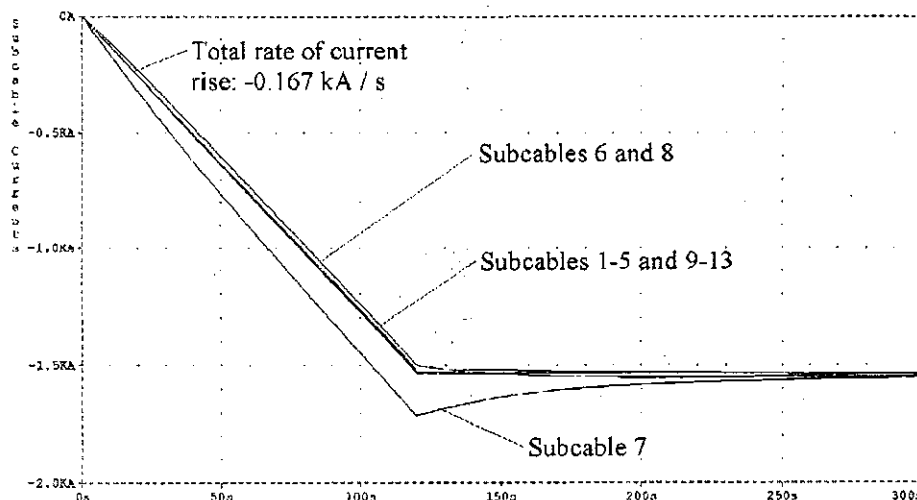


Fig. 5. Subcable currents after ramping up the POLO GKG cable to a current of - 20 kA in case of an unbalanced inductance matrix, contact resistances of  $30 \text{ n}\Omega$ , and a ten times slower total current rise rate than in Fig. 4

#### D. Numerical investigation of the effects of unequal contact resistances on the current distribution in the POLO GKG cable

The influence of a variance of the contact resistances of  $\pm 50\%$  is demonstrated in Fig. 6, 7, and 8. The simulations were performed with a symmetrical cable inductance matrix under

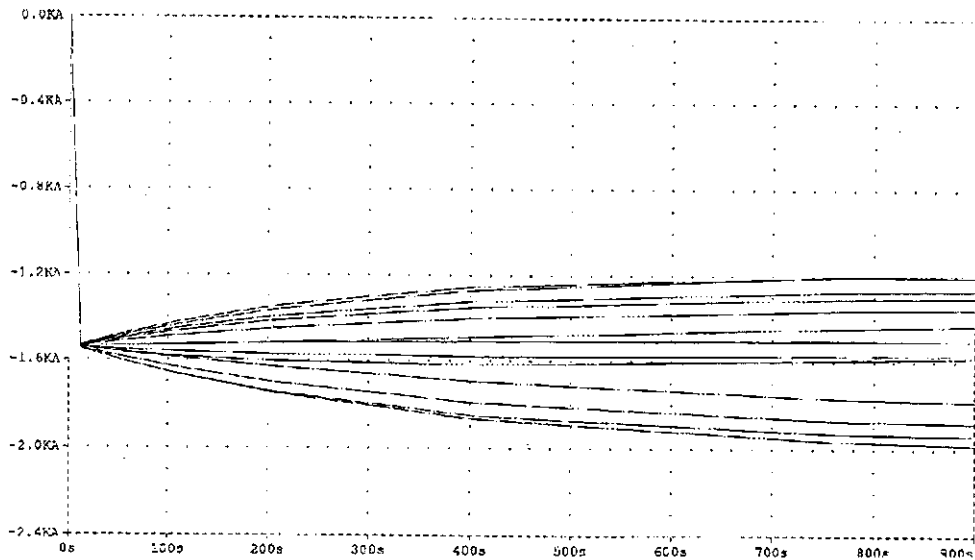


Fig. 6. Subcable currents after ramping up the POLO GKG cable to a current of -20 kA in case of unequal contact resistances ( $R_c = 3 \text{ n}\Omega \pm d$ ,  $d < 1.5 \text{ n}\Omega$ ) and a ramp rate of -1.67 kA/s, cable length about 10 m

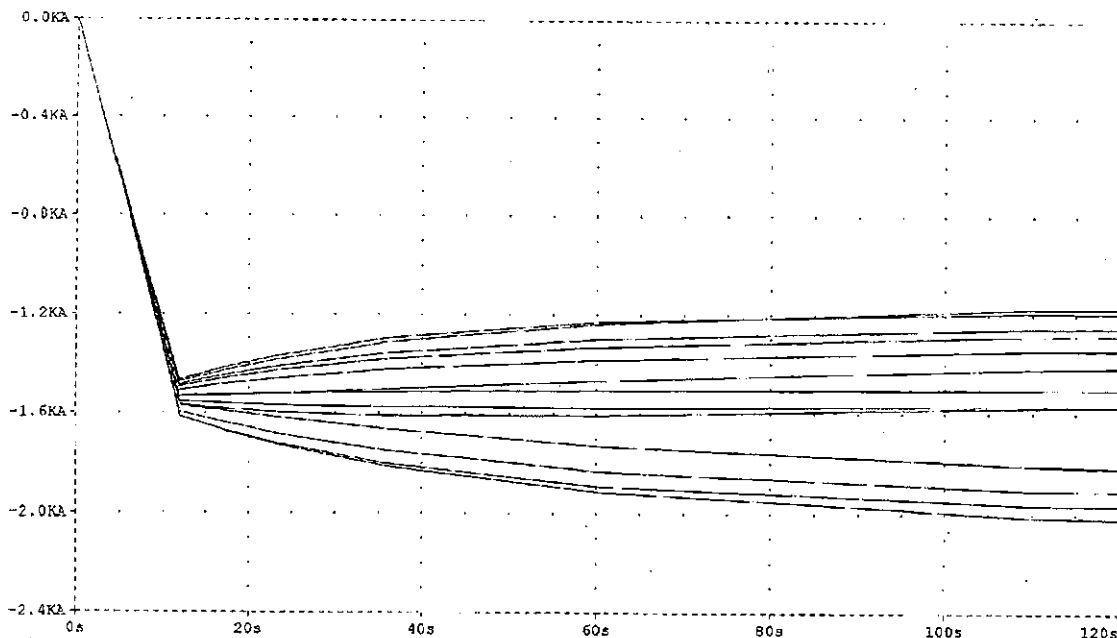


Fig. 7. Subcable currents after ramping up the POLO GKG cable to a current of -20 kA in case of unequal contact resistances ( $R_c = 30 \text{ n}\Omega \pm d$ ,  $d < 1.5 \text{ n}\Omega$ ) and a ramp rate of -1.67 kA/s, cable length about 10 m

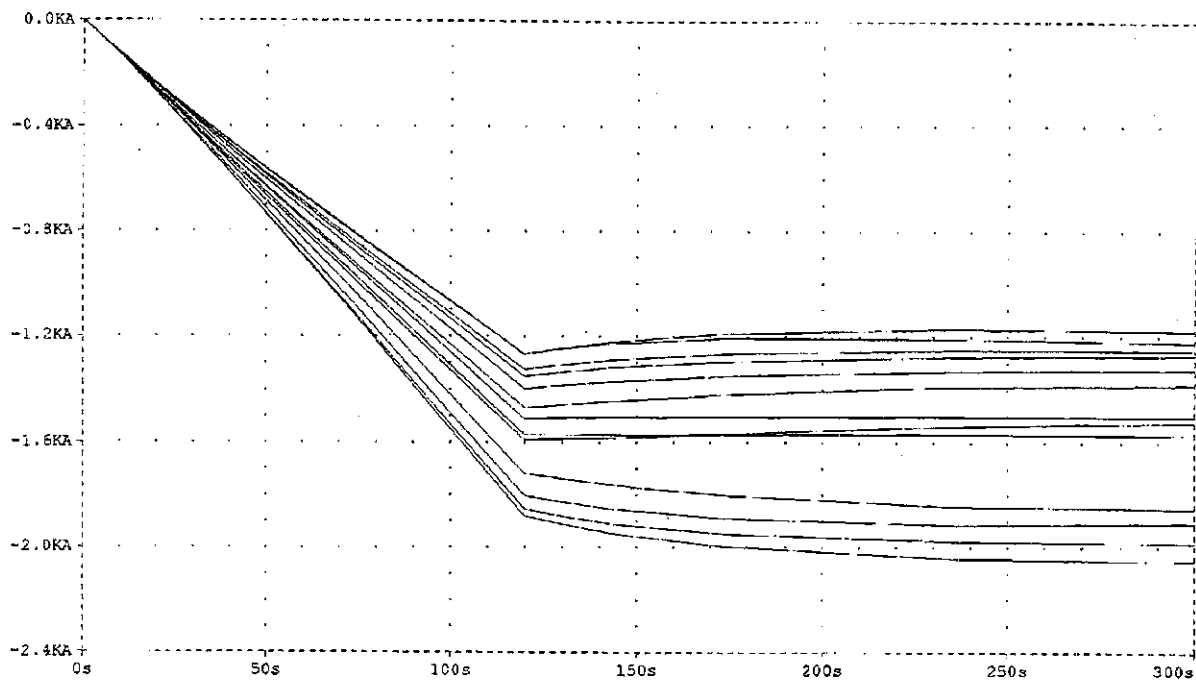


Fig. 8. Subcable currents after ramping up the POLO GKG cable to a current of -20 kA in case of unequal contact resistances ( $R_c = 30 \text{ n}\Omega \pm d$ ,  $d < 1.5 \text{ n}\Omega$ ) and a ramp rate of -167 A/s, cable length about 10 m

the assumption that all contact resistances  $R_c$  are subject to deviations in the resistance values. In case of Fig. 6 the contact resistances had values inbetween 1.5 n $\Omega$  and 4.5 n $\Omega$ . The contact resistance values used in case of Fig. 7 and 8 varied inbetween 15 n $\Omega$  and 45 n $\Omega$ . The final variance of subcable currents may be different in all three figures, because the deviations in the resistance values were accidentally scattered among all contact resistances  $R_c$  in Fig. 3.

### III. Investigation of subcable current distribution ramping up one half of the superconducting POLO coil

Due to the usually high inductance of magnet coils leading to long time constants in case of superconducting magnets, the influence of the contact resistances and total current rise rates on the subcable current distribution becomes negligible. Only the system inductance matrix has a perceptible effect on the current distribution after ramping. These statements can be made for coils being wound from cables with insulated and non-insulated strands and will be explained in this chapter by an electromagnetic model allowing the numerical analysis of the subcable current distribution in one half of the superconducting poloidal field coil POLO.

#### A. Electromagnetic model for the GKG half of the POLO coil

In the POLO coil the stainless steel jacketed conductor is wound in four double pancakes (DP 1 - DP 4, see Fig. 9). Each double pancake has 14 turns and is wound with a total length of 150 m. The conductor ends are brought together in the connection areas shown in Fig. 14 where the conductor terminals arise [23].

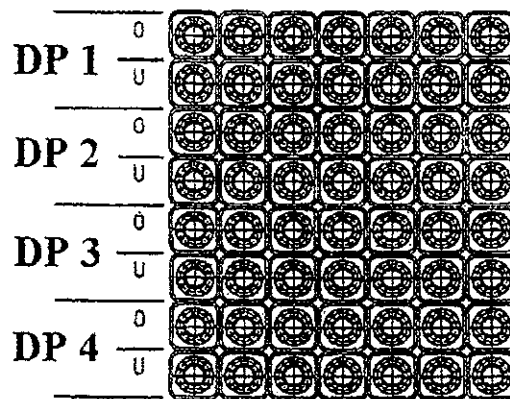


Fig. 9. Winding cross section of the POLO coil (the GKG half coil consists of DP3 and 4)

An electromagnetic model for the numerical analysis of the current distribution in the GKG cables must consider the magnetic couplings within the POLO cable and also the fact that all 28 turns in DP3 and DP4 are mutually coupled. At first the seven turns of one pancake were concentrated and regarded as one lumped inductance in order to reduce the computational effort involved with the coil. The magnetic couplings between these inductances were calculated with a pancake model having the same dimensions as the POLO winding and being composed of the four lower pancakes in Fig. 9.

Thus, the seven turns of each subcable in a pancake are regarded as one lumped inductance. That is rendered possible by the fact that all subcables in that half of the coil are electrically insulated from each other. However 2652 mutual inductances are involved with a simulation model consisting of 13 subcables in each of the four pancakes of the GKG half of the coil. But only 650 mutual inductances must be considered if a network model is used where each subcable in a double pancake is regarded as one lumped inductance. Such a model came into question for the investigation of current sharing during quench, since the measurement results were limited to the compensated subcable voltages in a double pancake. The magnetic couplings between the two halves of the coil do not show an effect on the results of these investigations. This will be explained in chapter IV in more detail. The good agreement of the calculated

and measured current sharing processes [10] actuated us to perform the analysis of RRL phenomena with the same type of model. Fig. 10 shows that model which also considers the contact resistances  $R_c$  at the double pancake joints.

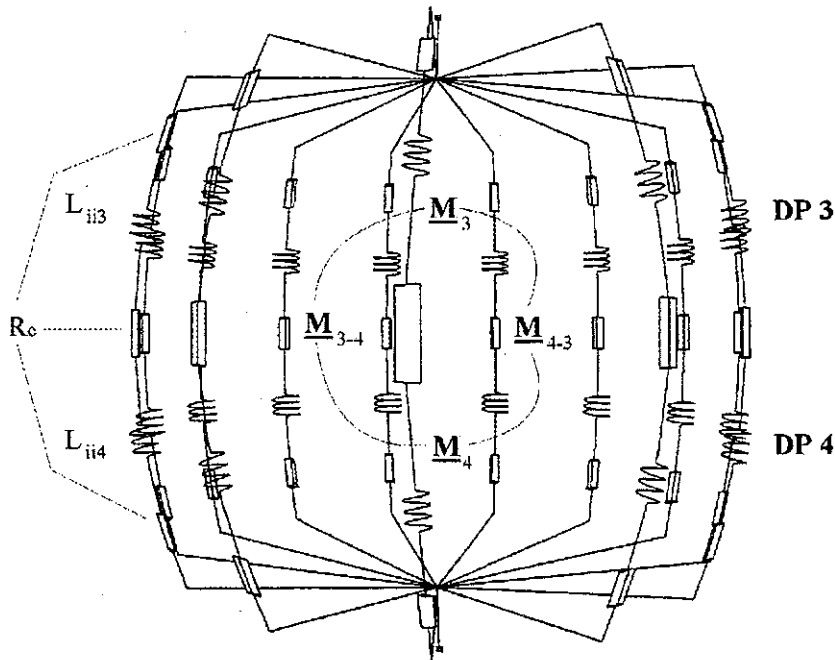


Fig. 10. Network model used for the analysis of current distribution in the GKG half of the POLO coil

The inductance values of the model were derived from calculations with the pancake model and from the cable inductance matrix of chapter II taking into consideration that each double pancake (DP) has 14 turns and that the mean value of the magnetic coupling factors ( $k = \frac{M_{ik}}{\sqrt{L_i L_k}}$ ) in a double pancake is 55 % [21]. That leads to values for the  $L_{ii}$  and  $M_{ij}$  that are 108 times higher than the corresponding values in the POLO cable model in Fig. 3, where each subcable inductance represents only one turn of the coil. The total inductance of the network model in Fig. 10 is 4.2 mH. That value for one half of the POLO coil corresponds well with the earlier calculated inductance of a POLO half coil of 4.6 mH [24].

Values of 3 n $\Omega$  were given to the contact resistances and the resistances to current leads  $R_c$ . These values lead to a total resistance over a double pancake joint of 0.46 n $\Omega$  which corresponds well with the value of about 0.5 n $\Omega$  measured during the POLO experiment [25].

### B. Numerical investigation of the effects of unequal contact resistances on the current distribution in the GKG cables of the POLO coil

The resistances of soldered subcable connections can vary for technical and also for geometrical reasons. Connecting 13 subcables to each other, it can not be excluded that the contact resistance values  $R_c$  might have tolerances up to 50 %. In order to get a quantitative comprehension of the influence of unequal subcable connections in a magnet it was assumed that the contact resistances  $R_c$  in Fig. 10 can be up to 50 % higher or lower than 3 n $\Omega$ , whereas the inductance matrix of the system is completely symmetrical. The variance of the  $R_c$  values was employed as described in section II.D. The main result of these simulations is shown in Fig. 11:

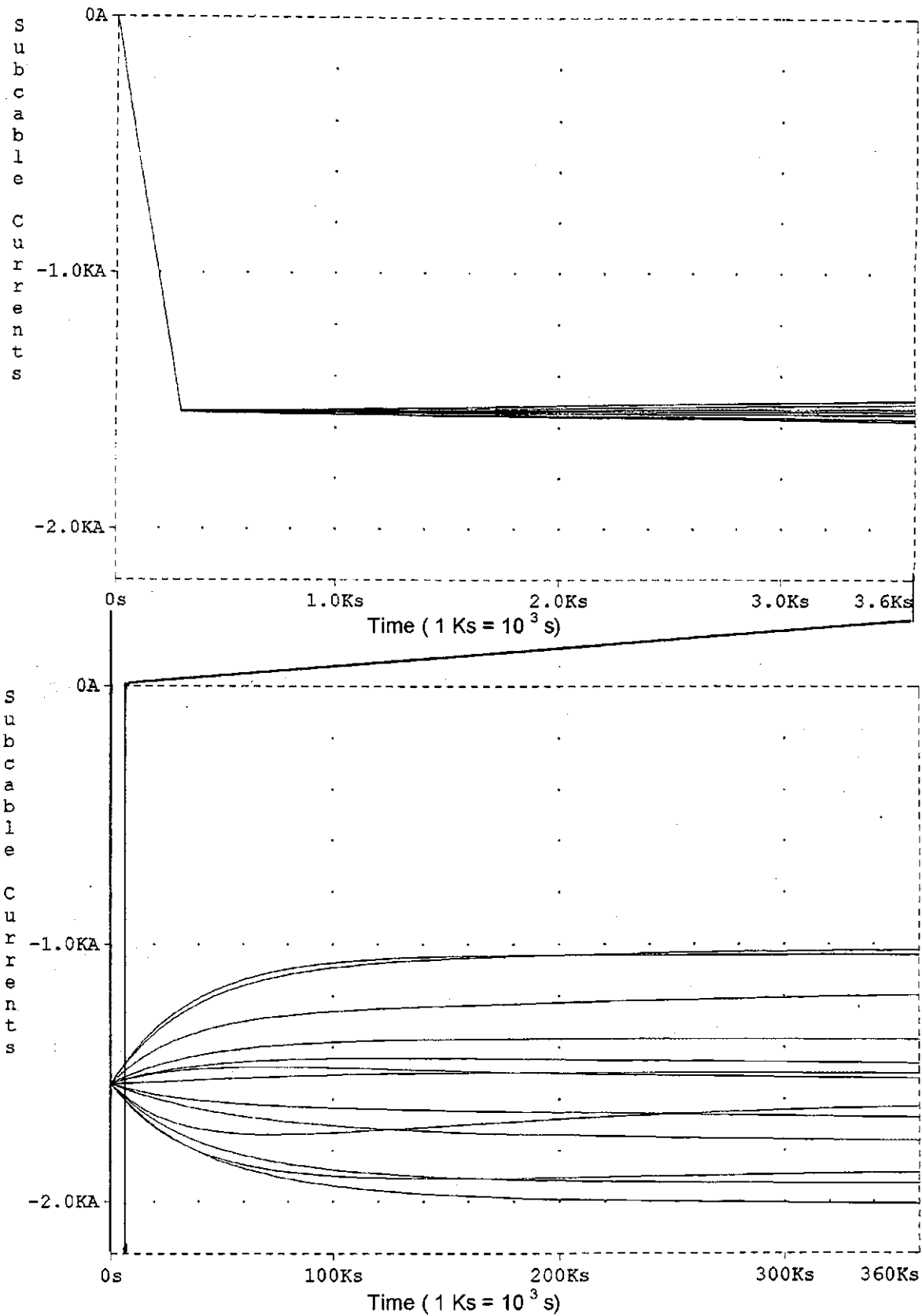


Fig. 11. Current distribution in the POLO GKG cable within the first hour (above) and within the first 100 hours (below) after ramping up half of the coil to a current of -20 kA (assumption: contact resistances vary up to 50 %)

As it was expected, the subcable currents show the same tolerances as the contact resistances  $R_c$ , but only after a very long time (in the range of 100 hours). Within the first hour after ramping up the coil the influence of unequal contact resistances is negligible.

**This result can be transferred to other superconducting magnets if they have parameters that are comparable to those of the POLO coil: It can be excluded that subcable connections with varying contact resistances (variance  $\leq \pm 50\%$ ) are responsible for RRL phenomena in such magnets.**

### C. Causes for unbalanced inductance matrices in superconducting magnets

On the one hand it can be excluded that unequal contact resistances cause perceptible inhomogeneous current distributions within the first hour after ramping up a superconducting coil. On the other hand it is obvious that the electromagnetic properties of the system are responsible for RRL phenomena. In this section causes for a disturbance of the subcable inductance matrix of a magnet will be discussed whereas the effects of such disturbances will be demonstrated in the following sections.

As emphasised before, minor disturbances in the symmetrical structure of a multistrand conductor result from cabling. Due to the mechanical strength of the cables the fabrication of long cable lengths is heavy duty mechanical engineering. Therefore minor deviations in the exact position of a subcable along the cable can hardly be prevented. The effect of such a tolerance depends mainly on the conductor concept. That statement can be explained looking at the magnetic properties of the POLO conductor in Fig. 12.

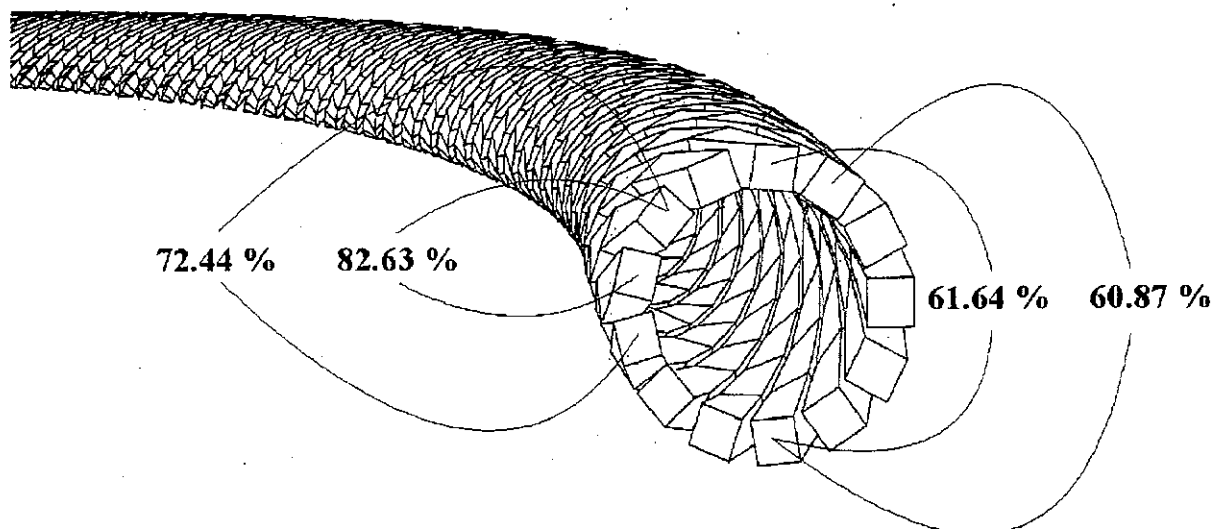


Fig. 12. Calculated values of the magnetic coupling factors ( $k = \frac{M_{ik}}{\sqrt{L_i L_k}}$ ) between adjacent and distant subcables

Changing the distance between two adjacent subcables (direct neighbours) by the same amount as between two subcables with a large distance from each other results in a change of the mutual inductances which is one order of magnitude higher in case of the adjacent subcables than

in case of the distant ones. That is an important fact that should be considered during the design stage of a conductor:

**The more direct (or near) neighbours a subcable has, the higher are the effects of displacements during the fabrication process on the symmetry of the cable inductance matrix. The displacement of subcables during the fabrication process has far less effects on the cable inductance matrix if each subcable has only two direct neighbours like in the POLO cable. Since small displacements during the fabrication process can not be prevented it should be emphasised that the POLO conductor concept is less critical for AC applications than, e.g., the Cable-in-Conduit-Conductor (CICC) concept.**

**The superconducting strands in the CICC concept are usually cabled with a multi-stage arrangement, the twisting of each single stage providing that no strands from one stage can stay in direct neighbourhood to strands from another stage along the conductor. But displacements within a stage (e.g., a quadruplet or a sextuplet) have more severe effects than in the POLO cable model shown in Fig. 12. The more stages are used, the higher are the variances that can occur in strand currents. The reason for that is that geometrical tolerances during cabling can occur in all stages. Therefore the process of compacting the transposed conductor is very critical with respect to the symmetry of the inductance matrix of CICC's.**

As illustrated in Fig. 1 the superconducting strands of the POLO conductor are cabled around a central CuNi wire in each subcable, in a first stage. But inspecting the conductor cross-section in different places it could be secured that no major changes in the position of the strands resulted from cabling.

An unbalanced cable inductance matrix can also be caused by a defect of one strand in a multistrand cable. Depending on the total number of strands and the position of the broken strand the effect of such a defect on the mutual inductances can be severe.

In superconducting coils disturbances of the symmetrical structure of the winding may occur for technical reasons. Fig. 13 which shows the joint of the POLO conductor and Fig. 14 showing the practical embodiment of such joints are examples for such disturbances. The POLO joint keeps the symmetry of the cable in that way that both cable ends are spliced and soldered together insulated from each other on a cylinder with two conical ends. Besides, the joint is screened by a copper cylinder to compensate the untwisted cable and weaken eddy current losses in the soldered subcable joints.

The not transposed cable sections in these areas are more critical than the change of the winding mutual inductances caused by the cable sections leading to the connection areas (see Fig. 14). The order of magnitude of asymmetry that such a joint can cause in the subcable inductance matrix can roughly be estimated comparing the length of the not transposed section with the total cable length in a DP:  $0.25 \text{ m} / 140 \text{ m} = 1.8 \text{ ‰}$ .

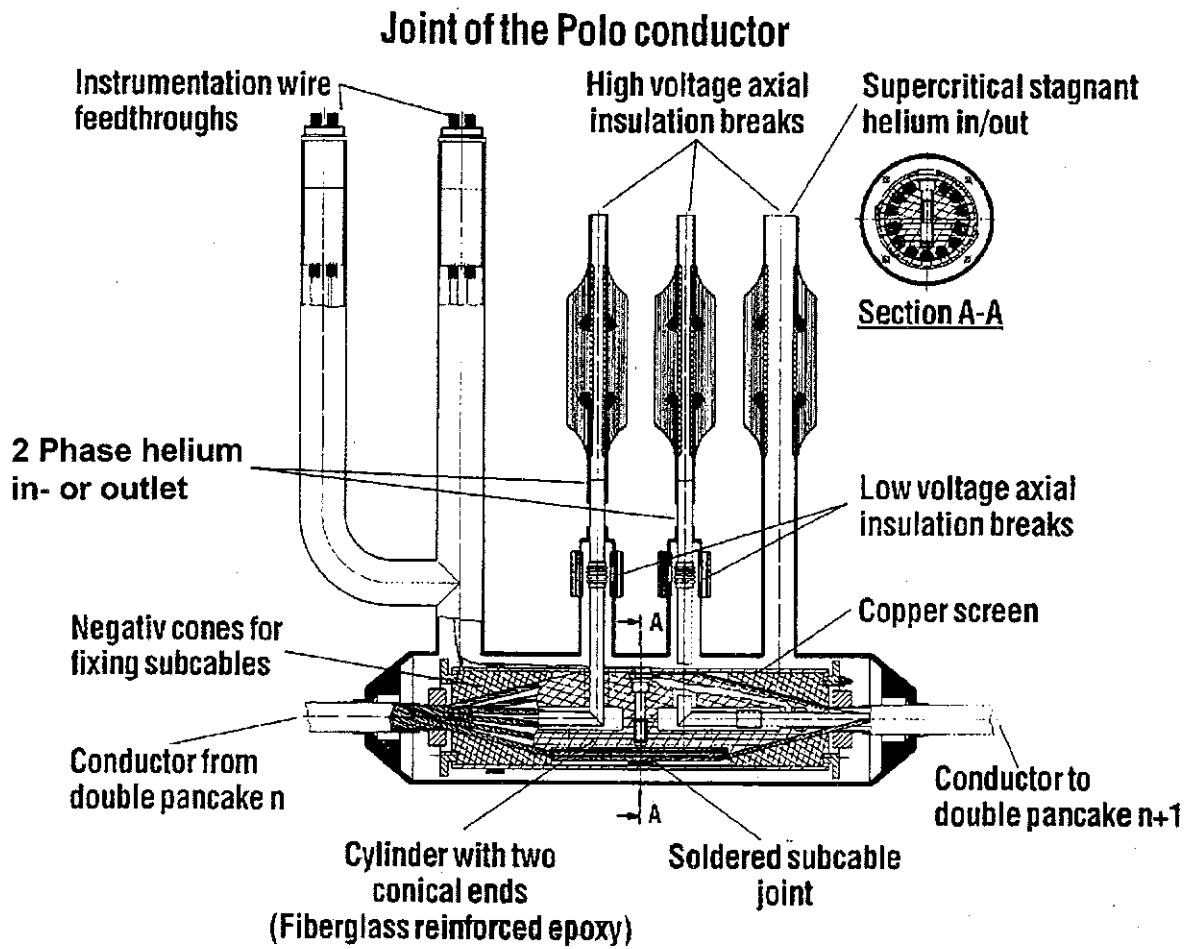


Fig. 13. Connection between double pancakes (not transposed cable length about 250 mm)

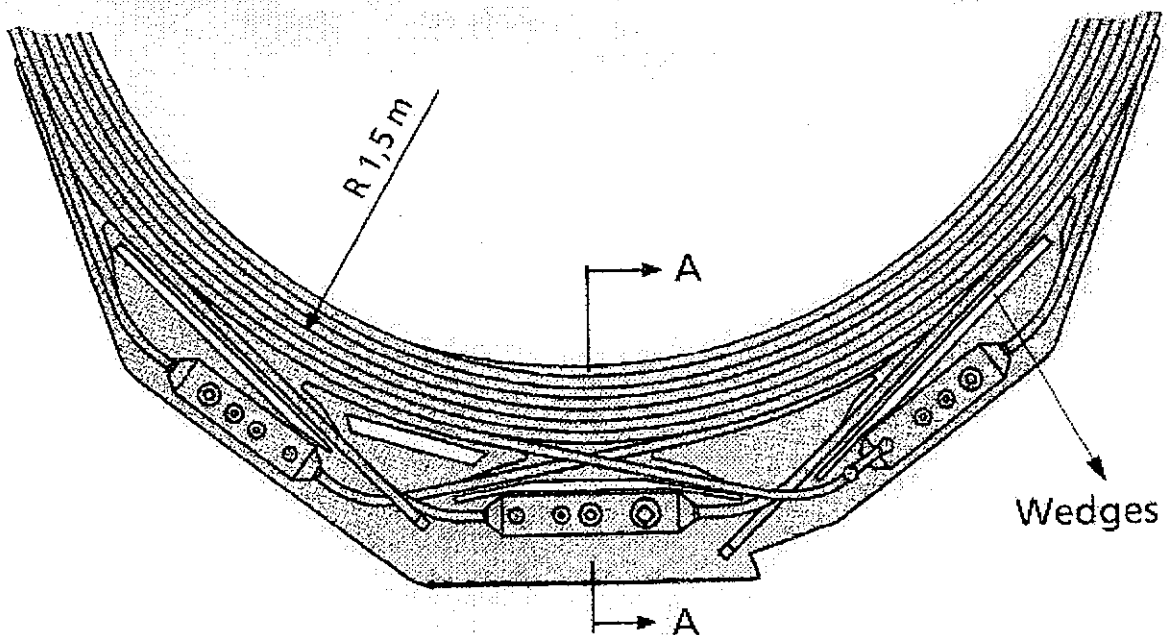


Fig. 14. Practical embodiment of the connections between double pancakes

#### D. Numerical investigation of the effects of an unbalanced inductance matrix on the current distribution in the GKG cables of the POLO coil

In order to be able to make quantitative statements on the effects of realistic disturbances in the symmetrical structure of a superconducting cable and winding (see section III.C), the following assumptions for the GKG half of the POLO coil were made:

1. Proceeding from the network model presented in Fig. 10 it was assumed that all contact resistances are equal
2. In a first step the symmetrical model inductance matrix derived in section III.A was manipulated assuming that 216 mutual inductances (which is about one third of all 650 magnetic couplings) are 1 % lower and 216 mutual inductances are 1 % higher than in case of an absolute symmetrical inductance matrix. These irregularities were scattered in the inductance matrix by means of a Fortran program in order to avoid any extreme accumulation of disturbances in a single subcable. Thus, it was assumed that the symmetrical structure of the **conductor and winding** are slightly disturbed (**case 1** of disturbance).
3. In a second step, it was assumed that only the symmetrical structure of the **conductor** is disturbed by such irregularities (**case 2** of disturbance) in order to be able to better understand the results from the first step.

**It should be emphasized that the order of magnitude of these disturbances is so small that they would not attract attention looking at a conductor with such irregularities with naked eyes. Even greater disturbances would not be visible in the direct neighbourhood of a subcable.**

The results of the simulations performed with the thus modified models are shown in Fig. 15, 16, and 17.

The thick line in the middle of the curves in Fig. 15 comes from a concentration of subcable currents around the current level  $I_m$  which is the current the subcables would have in case of a not disturbed inductance matrix. For many subcables, the disturbances scattered in the inductance matrix completely neutralise each other. But in other subcables, the disturbances are only partly neutralised. A more detailed explanation for the size of the variance of subcable currents will be given following Fig. 17 (**case 2** of disturbance). Since only the cable inductance matrix was modified in that case the corresponding simulation result can easier be explained.

Because of the long time constant of subcable current redistribution which is shown in Fig. 16 and Fig. 17, the ramp rate does not have a perceptible effect on the variance of subcable currents in such a magnet.

As it was expected from the number of manipulated magnetic coupling factors, the variance of subcable currents in **case 2** (Fig. 17) has only about half the size of the variance of subcable currents in **case 1** (Fig. 16).

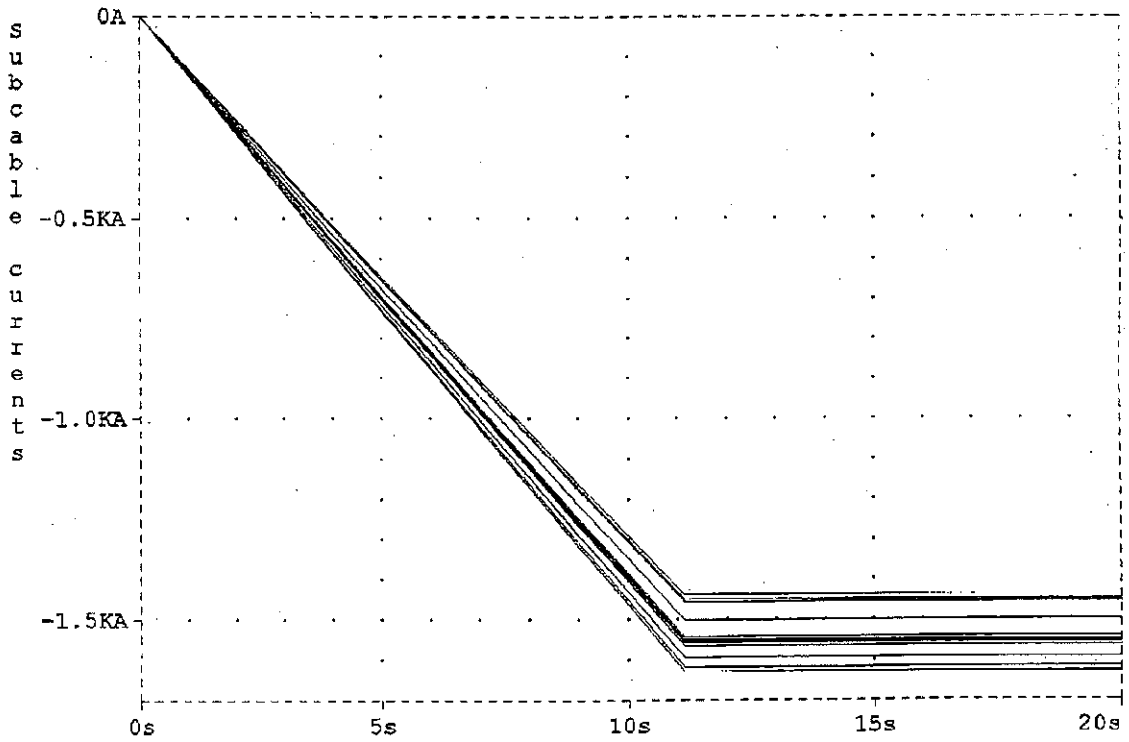


Fig. 15. Current distribution in the POLO GKG cable ramping up half of the coil to a current of -20 kA (assumption: variance of the  $M_{i,k}$  values along the winding of 1‰ - case 1 of disturbance)

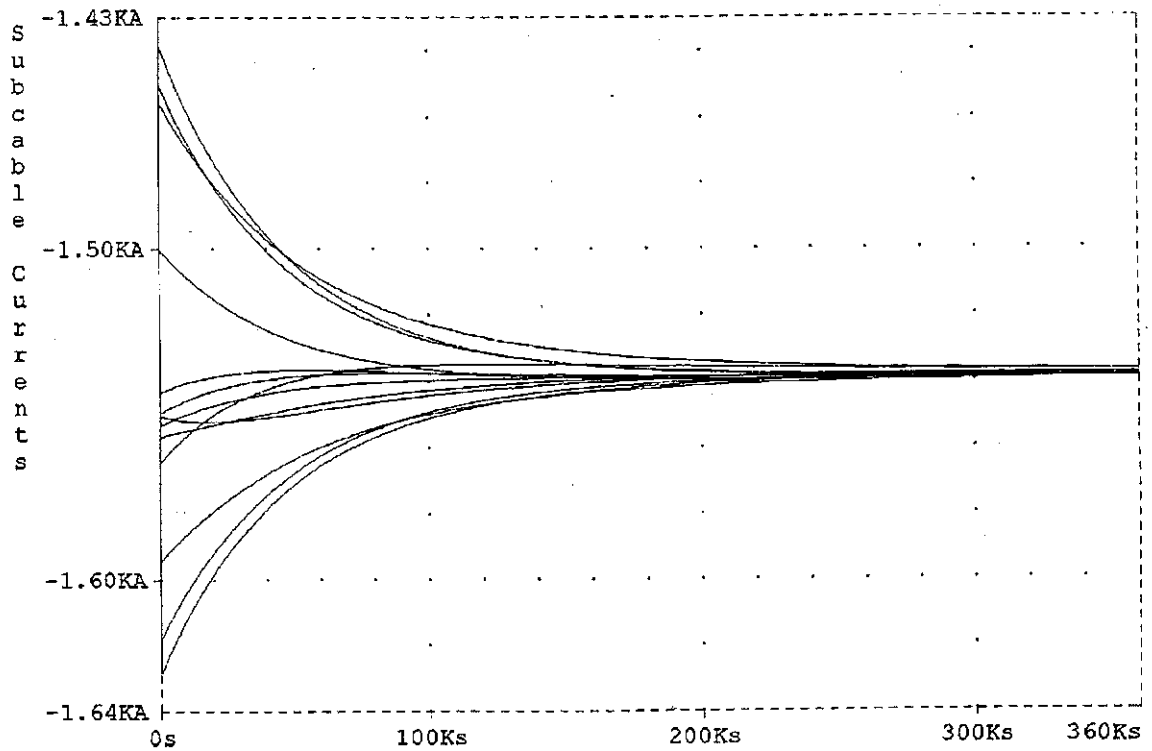


Fig. 16. Current distribution in the POLO GKG cable in the first 100 hours after ramping up half of the coil to a current of -20 kA (assumption: variance of the  $M_{i,k}$  values along the winding of 1‰ - case 1 of disturbance)

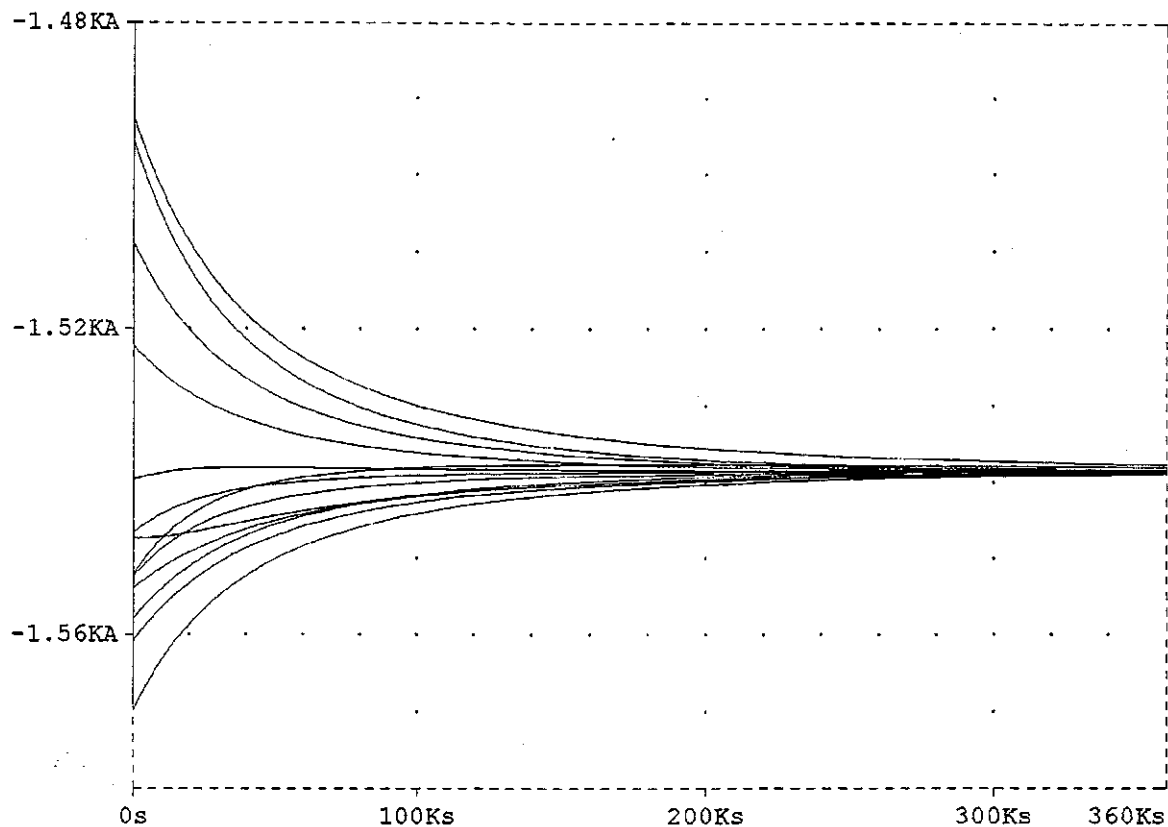


Fig. 17. Subcable currents in the POLO GKG cable in the first 100 hours after ramping up half of the coil to a current of -20 kA (assumption: variance of the  $M_{i-k}$  values within the cable of 1 ‰ - case 2 of disturbance)

After the numerical manipulation in case 2 the cable inductance matrix was checked in order to find out what the highest grade of magnetic asymmetrie is, the manipulation has caused for a single subcable. Considering that there are 24 magnetic couplings of one subcable to all other subcables and that each of these couplings could be increased or decreased by 1 ‰ by the manipulation, the maximum change in the **total** magnetic coupling a single subcable ended up with was 1.6 ‰. However, the current in that subcable differs by 3.2 ‰ from  $I_m$ , which is the current the subcables would have in case of a not disturbed inductance matrix.

That can be explained calling back to mind the reason for the high variance of subcable currents in the preliminary, analytical example in section II.B. Although the magnetic coupling of subcable 7 to all other subcables was changed by altogether 24 ‰ in that example, the current in that subcable changed by 34 ‰. That value was analytically derived and is caused by the currents in the neighboured subcables, although their inductance values were not changed at all.

In the here described simulation, it must be considered that the mutual inductance values of the neighboured subcables also might have been changed by the manipulation which leads to a much higher degree of disorder than in the preliminary, analytical example. Therefore, a change in the value of a subcable current of 3.2 ‰ can occur even though the total magnetic coupling of that subcable was changed by only 1.6 ‰. In the following paragraphs that effect will be referred to as "**Intensification by Lenz's Law**", abbreviated **ILL**. The occurrence of that effect is not specific for the POLO cable. The ILL effect also has negative influences on the current distribution within each stage (triplet, quadruplet, ... ) of a CICC.

**A variance in the subcable currents of CICC's which is many times higher than the ones shown in these figures can be explained by geometrical irregularities within such conductors for the reasons pointed out on page 19.**

Increasing RRL phenomena were observed with increasing ramp rates in cable experiments, as in the measurements performed using a 27 strand CICC extracted from the 225 strand US-DPC cable [7]. The statement that the ramp rate does not have a perceptible effect on the current distribution in the here performed simulations seems to be contradictory to this. But both observations agree well with each other taking into consideration that:

1. Cable experiments are performed with short lengths. In the simulations performed with a 10 m long POLO cable (see section II.C), it was observed that the variance of the subcable currents strongly increases with increasing ramp rates. That effect is demonstrated in Fig. 4 and Fig. 5.
2. The simulations performed in this paper do not take into account the effect of the coupling losses which are proportional to  $\dot{B}^2$ . Their influence superposes the effects caused by geometrical irregularities or the space dependence of  $\dot{B}$ , which are not ramp rate dependent effects. It is therefore clear that RRL phenomena in magnets with geometrical irregularities are ramp rate dependent.

**In cable experiments with short lengths the electrodynamics of subcable current distribution differ by orders of magnitude from the electrodynamics of subcable current distribution in a magnet. Even major disturbances in the symmetrical structure of the cable may therefore only become visible in such experiments if high ramp rates are used.**

#### **E. Influence of a transverse conductivity between subcables on the current distribution in the cables of the POLO coil**

In non-insulated strand cables the current redistribution locally occurs around the normal spot when a quench is initiated in one strand (see section IV.B). In this section the case of inhomogeneous current distributions in such cables without occurrence of a quench will be analysed using a simple model for the transverse conductivity.

In that case the answer to the question whether the current redistribution occurs locally or by superposed currents flowing over long lengths mainly depends on the size of the transverse conductivity and on the size of the contact resistances to current leads [9]. As emphasized in section III.C, the inductance matrix of a magnet always has slight irregularities. In order to get a qualitative understanding for the influence of transverse conductivity in such a magnet and in order to be able to make quantitative statements on the losses in the connection area between double pancakes in case of a joint where all subcables are soldered together (in contrast to the double pancake joint shown in Fig. 13), the network model shown in Fig. 18 was used.

In that model the contact resistances  $R_c$  between  $L_{ii3}$  and  $L_{ii4}$  (see Fig. 10) are not considered any longer because their influence is negligible in the here performed simulations.

At the double pancake connection in Fig. 18 all subcables are connected to each other by 13 ohmic resistances  $R_{trans}$ .

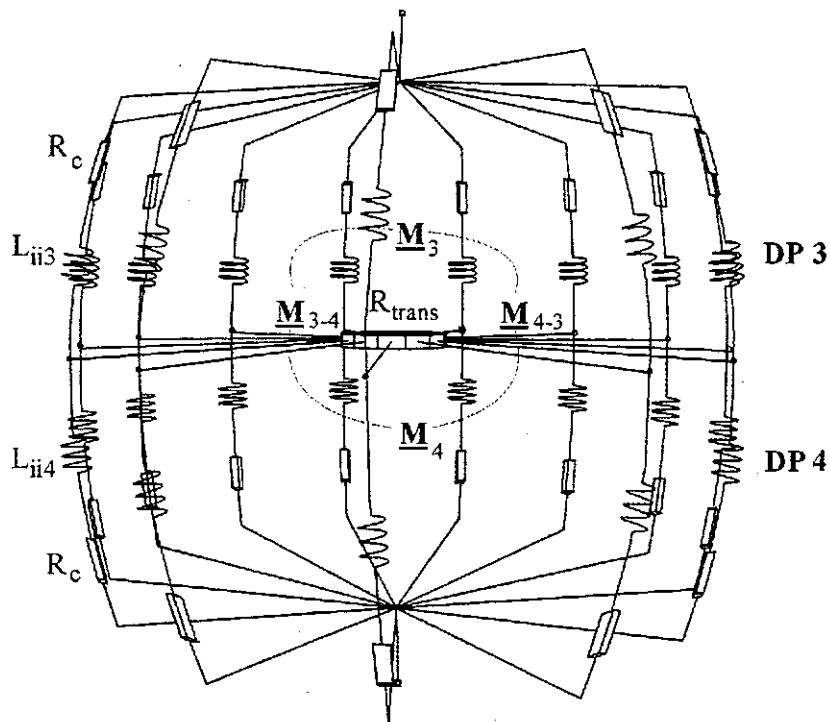


Fig. 18. Modification of the model for the GKG half of the POLO coil by introduction of a lumped transverse conductivity at the double pancake connection

In a first step simulations were performed with this model proceeding from an inductance matrix with the slight irregularities described on page 21 (case 1 of disturbance) and values for the transverse resistances  $R_{trans} = 3 \text{ n}\Omega = R_c$ . Thus it was assumed that the transverse resistivity at the double pancake connection is as low as the resistivity to the current leads. The main result of that simulation is shown in Fig. 19.

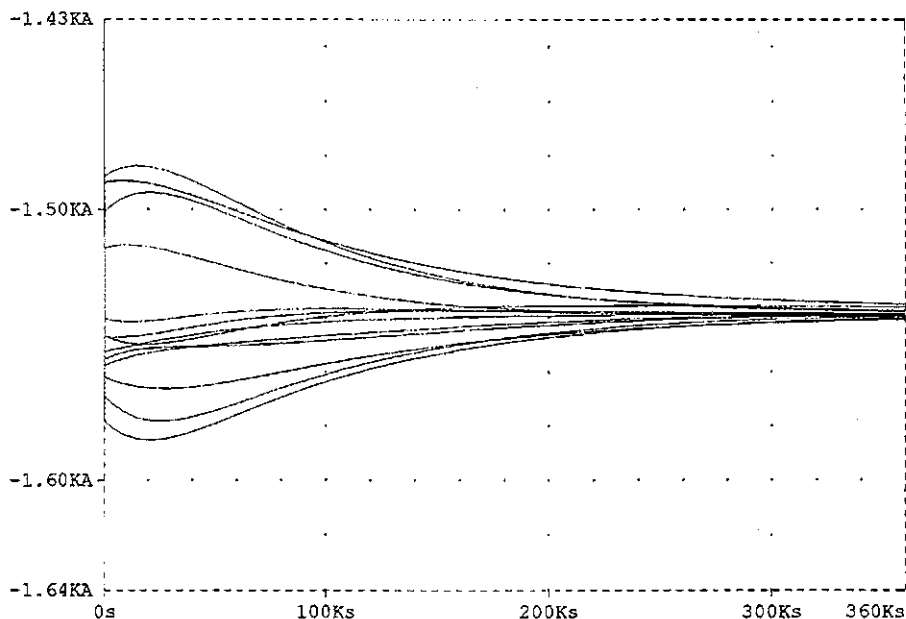


Fig. 19. Subcable currents in the POLO half coil model with lumped transverse conductivity after ramping up to a current of -20 kA (assumption: variance of the  $M_{i-k}$  values along the winding of 1‰ - case 1 of disturbance)

As it was expected, the transverse conductivity causes a subcable current distribution which is not as inhomogeneous as shown in Fig. 16 directly after ramping up. But some subcable currents reach their maximum value only several hours after ramping up. Then the variance of subcable currents is about the same as in Fig. 16 at that time.

Such increasing or decreasing amplitudes of single subcable currents with very long time constants were experimentally observed in magnets after charging [9]. The increasing subcable currents in Fig. 19 endanger the long term magnet stability since they can cause a quench many hours after charging a magnet although no external parameters are changed.

The transient behaviour of the subcable currents in Fig. 19 can be explained by currents being interchanged between subcables. These intercable currents which are shown in Fig. 20 flow over the transverse resistances  $R_{\text{trans}}$  in the network model illustrated on page 25. The electro-dynamics leading to the intercable currents are caused by slightly different irregularities in the inductance matrices of DP3 and DP4.

Multiplying the intercable currents with the respective voltages across the 13 transverse resistances  $R_{\text{trans}}$  leads to the ohmic losses caused at such a double pancake joint. The maximum loss across a single transverse resistance  $R_{\text{trans}}$  is shown in Fig. 21. The total ohmic losses at the double pancake joint would be smaller than 13 times the loss values traced in Fig. 21.

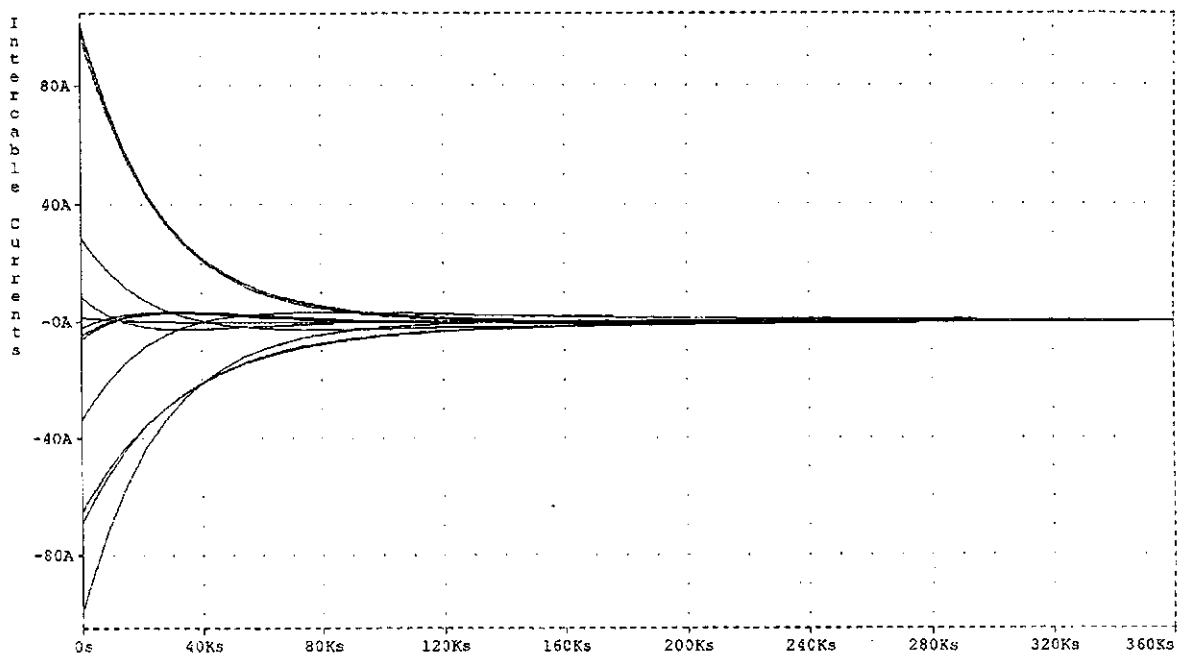


Fig. 20. Currents flowing across the 13 transverse resistances  $R_{\text{trans}}$  in the POLO half coil model with lumped transverse conductivity after ramping up to a current of -20 kA (same simulation as in Fig. 19)

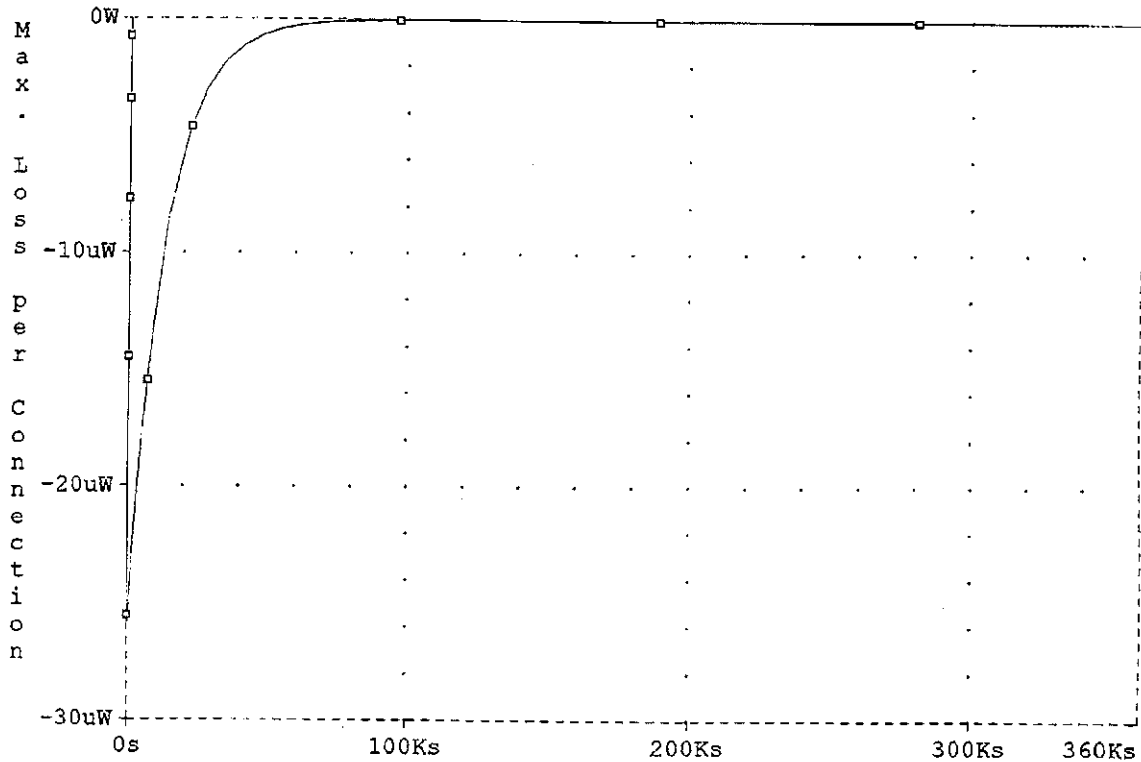


Fig. 21. Maximum loss in a single transverse resistance  $R_{trans}$  in the POLO half coil model presented in Fig. 18 (same simulation as in Fig. 19)

That means: If a variance of the  $M_{i,k}$  values along the winding of 1 ‰ is assumed so that intercable currents of altogether more than 600 A flow through the normal conducting connection area, the losses caused by intercable currents in that joint would stay below 350  $\mu\text{W}$  at any point of time.

**It can therefore be excluded that a thus realised double pancake joint (see page 24) has a remarkable negative influence on the stability of a magnet with parameters that are comparable to those of the POLO coil.**

In a second step it was assumed that only the inductance matrix  $\underline{M}_3$  of DP 3 in Fig. 18 has little irregularities, whereas no other irregularities occur in the half coil model. That assumption was made in order to estimate the effects of such a locally restricted defect on the performance of a magnet with transverse conductivity. The grade of irregularity is the same as the one described on page 21 (case 2 of disturbance). The subcable currents after charging the half coil model under these assumptions are shown in Fig. 22 for a transverse resistance  $R_{trans} = 3 \text{ n}\Omega = R_c$  and in Fig. 23 for transverse resistances  $R_{trans} = 30 \text{ n}\Omega = 10R_c$ .

As it was expected, the subcable currents in Fig. 22 and 23 have

- the same initial value in DP 4 which is the current the subcables would have in case of ideal conductors and an ideal winding
- the same initial variance in DP 3 which has about the same size as in Fig. 17
- the same final values after more than 100 hours
- different time histories.

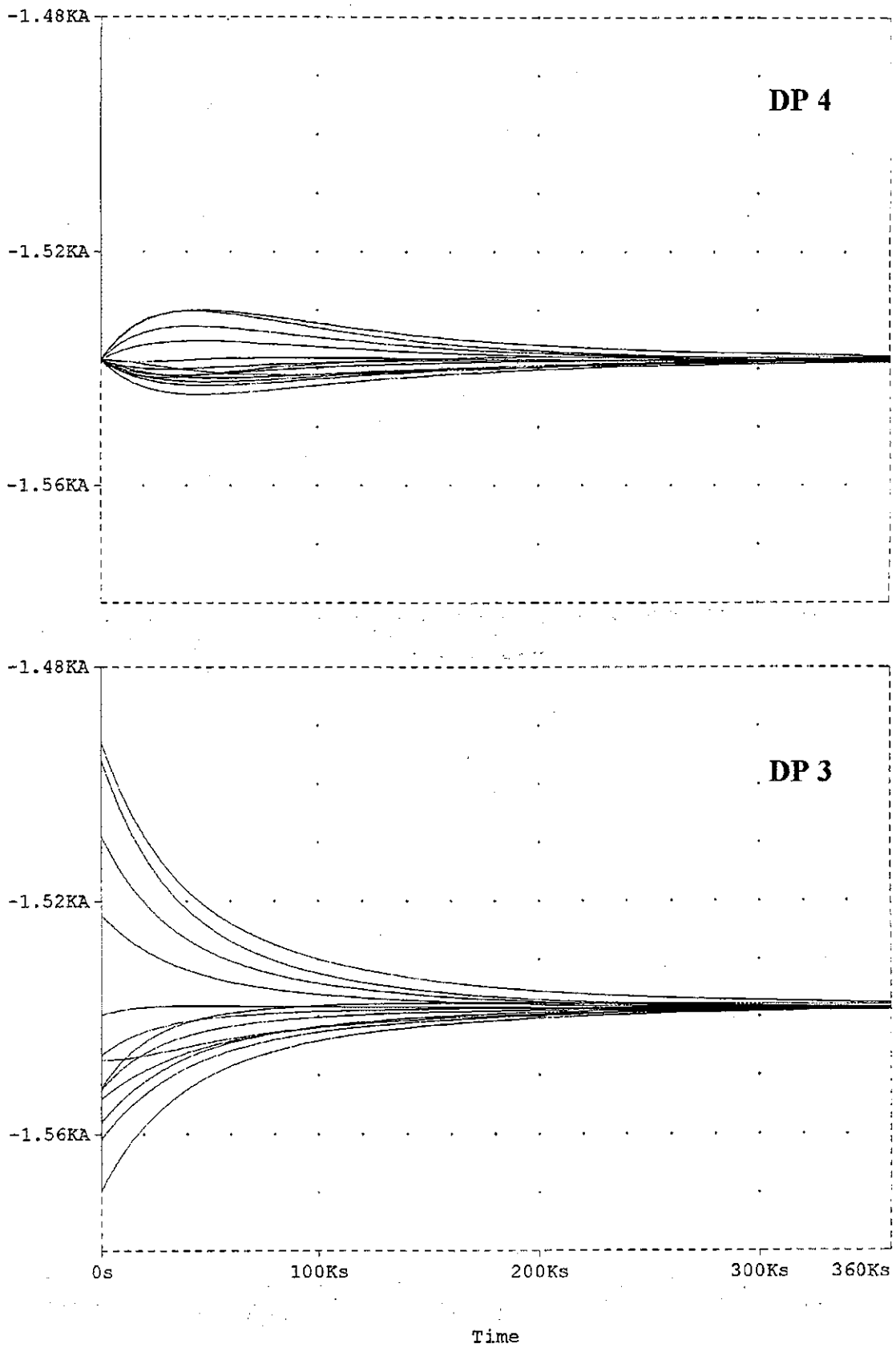


Fig. 22. Subcable currents in the POLO half coil model with lumped transverse conductivity after ramping up to a current of -20 kA (assumption: **variance of the  $M_{i,k}$  values only in the conductors of DP 3,  $R_{trans} = 3 \text{ n}\Omega = R_c$** )

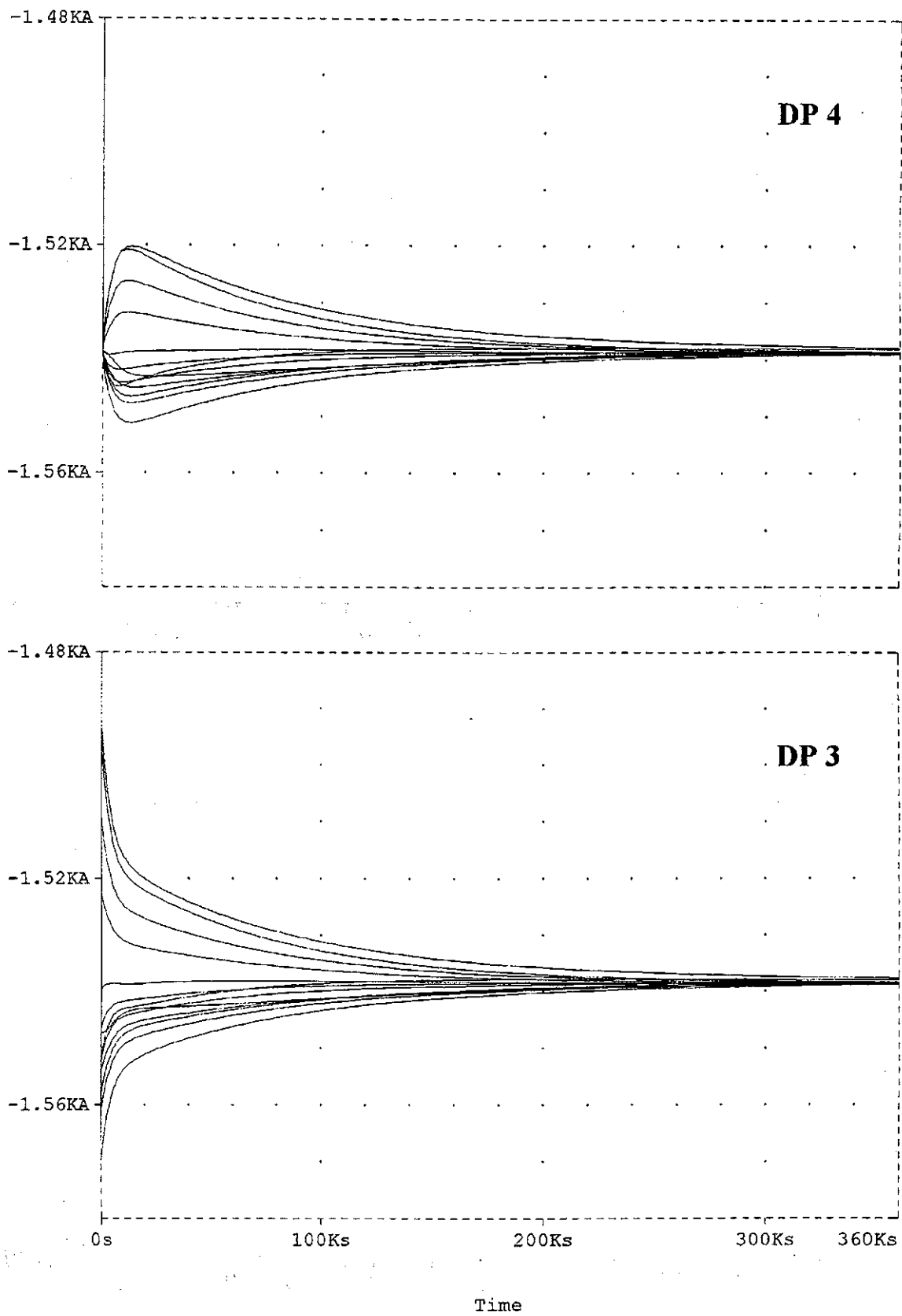


Fig. 23. Subcable currents in the POLO half coil model with lumped transverse conductivity after ramping up to a current of -20 kA (assumption: **variance of the  $M_{i-k}$  values only in the conductors of DP 3**,  $R_{\text{trans}} = 30 \text{ n}\Omega = 10R_c$ )

Whereas in Fig. 22 the current redistribution after charging has not many consequences for the subcable currents in DP 4, it can clearly be recognized in Fig. 23 that after about six hours (21600 s) the subcable currents in DP 3 and DP 4 are exactly the same. Only at the beginning of the electrodynamic process of current redistribution currents flow across the transverse resistances  $R_{\text{trans}}$

The time constants of the intercable currents in Fig. 23 which are one order of magnitude smaller than the ones in Fig. 22 can be explained by the ten times higher transverse resistances in that simulation. The time constant of the electrodynamic process of current redistribution is inversely proportional to the resistance of the intercable current path with the best conductivity. In Fig. 23 that intercable current path is the path over the contact resistances to the current leads. Therefore the electrodynamic process of current redistribution is only at the beginning influenced by transverse conductivity in that simulation. Already after a fraction of the period of current redistribution the transverse conductivity has no more effects and the inhomogeneity of subcable currents is the same in DP3 and DP4.

In order to be able to transfer the simulation results from models with lumped transverse conductivity to a non-insulated strand winding as, e.g., the CuNi half of the POLO coil, where the transverse conductivity is distributed along the subcables, the following properties of the CuNi subcables and POLO winding must be considered:

- the transverse resistance between neighbouring subcables is about  $6 \mu\Omega$  per meter [26 ]
- the total length of two double pancakes is  $2 \times 150 \text{ m} = 300 \text{ m}$

From these data follows that the total transverse resistivity between the subcables of a double pancake has the same order of magnitude as in the simulation performed with the transverse resistances  $R_{\text{trans}} = 30 \text{ n}\Omega$ . For that reason it may be assumed that the CuNi half of the POLO coil would react similar as shown in Fig. 23 to disturbances in the cable or winding inductance matrix.

The simulations were performed with a relative simple model which does not consider that the transverse conductivity is distributed along the subcables of the CuNi half of the POLO coil. But since the transverse conductivity along the subcables is in the range of  $\mu\Omega$  per meter, it may be excluded that this transverse conductivity causes a dynamic subcable distribution that differs remarkably from the one shown in Fig. 23.

The effects of disturbances in the inductance matrix of the CuNi half of the POLO coil can therefore be concluded as follows:

1. Directly after charging, the variance of subcable currents in the CuNi cables is not remarkably lower than in case of cables with insulated strands (compare Fig. 17 and DP3 in Fig. 23)
2. The higher the ratio of the distributed transverse resistivity to the resistivity across the current lead is, the shorter and minor is the influence of the distributed transverse conductivity on the period of current redistribution. In case of the CuNi half of the POLO coil the subcable currents in DP3 and DP4 are the same after a fraction of that period (see Fig. 23), although all irregularities in the subcable inductance matrix were locally restricted to DP 3.

**That demonstrates clearly that minor irregularities along a cable with non-insulated strands can lead to major supercurrents [3-4, 9] flowing over the whole cable length of a magnet after a relative short period of time. The size of these supercurrents is hardly influenced by the transverse conductivity distributed along the subcables, as long as that transverse conductivity is small compared to the conductivity to current leads.**

**Only high transverse conductivities between subcables (as in Fig. 22 or in Fig. 19) have a positive influence on the homogeneity of current distribution after ramping. But in magnets being wound from conductors with sufficient transverse conductivity between the subcables the ramp rate is limited due to the coupling losses.**

## IV. Current sharing during quench of the POLO coil - results of calculation and measurement

### A. Quench in the GKG half of the POLO coil

The calculations were performed with the network model for the GKG half of the POLO coil which is shown in Fig. 10. That model can be used for a detailed simulation of current sharing processes, since the GKG cables have no transverse conductivity. The mutual inductances with the CuNi half of the POLO coil are not considered in these simulations. However accurate results for the current sharing processes are to be expected from the model in analysing cases where the measured coil current was constant during the current sharing process. Thus the mutual inductances with the other half coil can be neglected at these times. The resistive zones were modelled by time dependent ohmic resistances. In accordance with measurements these resistances were defined that way that a smooth (exponential) resistance rise in quenching subcables occurs. The rates of resistance rise were based on measurements performed during quench of the POLO coil, where rise rates in the range of  $1 \text{ m}\Omega/\text{s}$  were measured about 200 ms after quench initiation (see Fig. 27-29). All simulations in chapter IV are performed with undisturbed inductance matrices and equal contact resistances.

#### 1. Quench in only one subcable of the GKG half

In order to determine the effective time constants for the current sharing process in the GKG cable, a resistive zone of length  $l = 25 \text{ m}$  = constant in only one subcable was assumed. The result of that simulation is shown in Fig. 24.

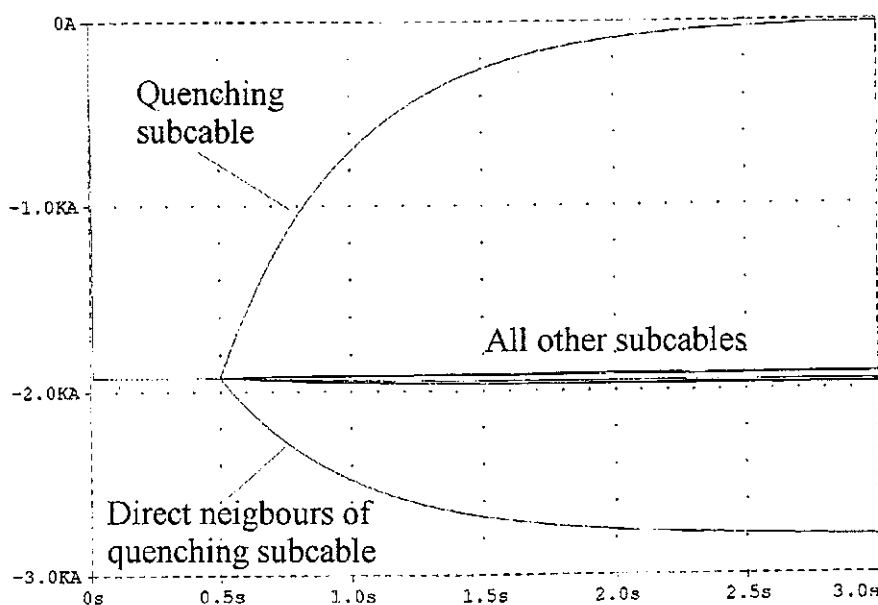
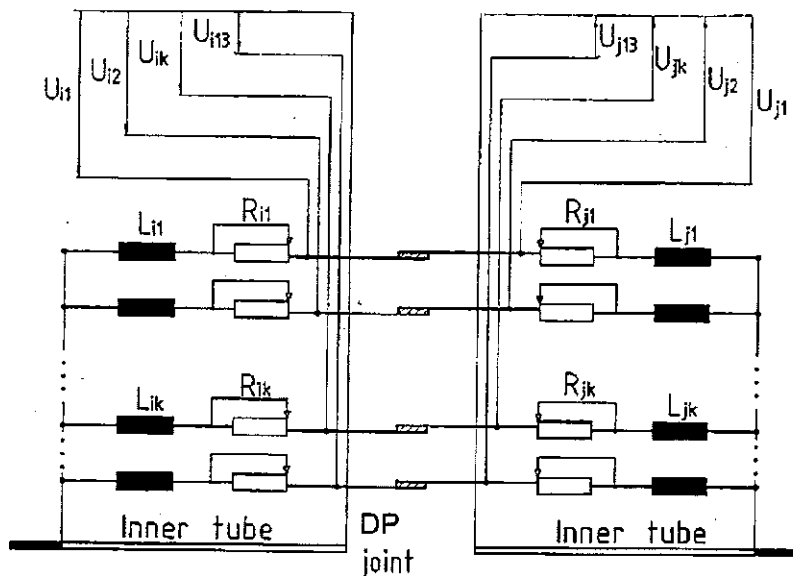


Fig. 24. Subcable currents during quench in only one subcable of the POLO GKG conductor (assumption: resistive zone of length  $l = 25 \text{ m}$  = constant in that subcable, corresponding ohmic resistance:  $1.1 \text{ m}\Omega$ )

The subcable current in the quenched subcable decreases to zero with a time constant of 595 ms. The time constant is much higher if one proceeds from a more realistic quench process in which the quench zone slowly starts growing and reaches values in the range of 1 m $\Omega$ /s only after about 200 ms. It is therefore clear that no recovery can occur in the GKG half of the POLO coil if a quench is initiated in one subcable. As it was to be expected from the simulations performed in section II and III, the current from the quenching subcable is mainly transferred to its two direct neighbours.

The measurement of the current sharing processes during the POLO experiment was performed by means of compensated voltages. They were measured as shown in Fig. 25.



$L_{ik}, L_{jk}$  : Subcable inductances ( $k = 1 \dots 13$  subcable index),  $i$  and  $j$  DP index ( $i, j = 1 \dots 4$ )  
 $R_{ik}, R_{jk}$  : Resistive zone representation ;  $U_{ik}, U_{jk}$  : Compensated voltages

Fig. 25. Equivalent POLO cable network for two double pancakes (DP's) with voltage taps for measuring the compensated voltages

Besides the subcable currents also the compensated voltages were determined in simulating the quench process, in order to check the validity of the simulation results. The compensated voltages that would, e.g., result from the simulation in Fig. 24 are shown in Fig. 26.

The compensated voltage in DP 4 of the quenched subcable consists of an ohmic and an inductive portion, whereas the compensated voltage in DP 3 of that subcable and the compensated voltages of all other subcables are only inductive. The inductive voltage in DP 3 of the quenching subcable is much higher and has different polarity than all other purely inductive voltages, because that voltage is mainly caused by the decreasing current in the quenching subcable. The inductive voltage in all other subcables results mainly from increasing currents. The voltage across the resistive zone  $U_R$  can be obtained from the curves of the quenched subcable in adding the compensated voltages of DP 3 and DP 4 together. Since all subcables are soldered together at the terminals (see Fig. 25) it is clear that the voltage  $U_R$  also appears across the two double pancakes of the subcables that remained superconducting. In these subcables the voltage  $U_R$  is caused by the inductive coupling caused by current sharing. The voltage drop across a DP in these subcables is  $0.5 U_R$ .

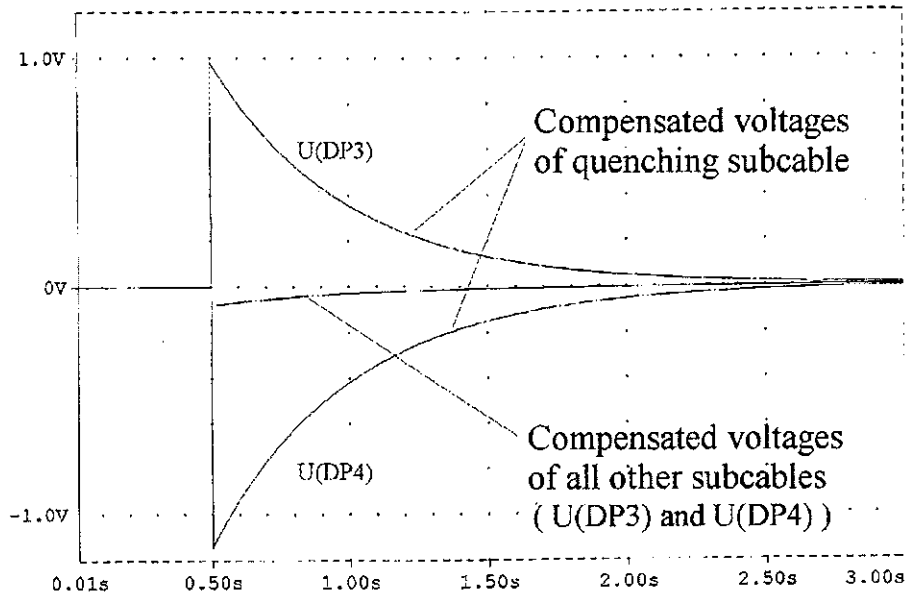


Fig. 26. Calculated compensated voltages of all subcables during quench in only one subcable of the POLO GKG half (assumption: resistive zone of length  $l = 25 \text{ m} = \text{constant}$  in that subcable, corresponding ohmic resistance:  $1.1 \text{ m}\Omega$ , quench in DP 4)

Simulations were performed with the model of quench propagation described above in order to find out which amplitudes of  $U_R$  must be expected in case of a realistic quench propagation. The result is that if only one subcable becomes normal conducting and all others stay superconducting, the ohmic voltage across the quench zone would start at  $0 \text{ V}$  and reach less than  $2 \text{ mV}$  after  $100 \text{ ms}$ .

That result is important with respect to the measured compensated voltages during the POLO experiment: Cases where not all subcables quench, but at least one subcable stays superconducting, can be recognized by the existence of compensated voltages that stay practically zero (below  $2 \text{ mV}$ ) during the first  $100 \text{ ms}$ .

## 2. Quench in all subcables of the GKG half - comparison of calculated and measured results

Since no recovery can occur in the GKG half of the POLO coil, all compensated voltages measured during quench in DP3 or DP4 originate from quenches where all subcables went normal.

As explained in section IV.A.1, the simulated and measured quench process shown in Fig. 27 is a quench where not all subcables quench at the same time. Similar compensated voltage patterns were also measured in case of quenches at other current levels or in case of quenches following a half-coil discharge [10]. The subcables become normal conducting in that quench one after another. A time period between quench initiation in the first and quench initiation in the last subcable of less than  $30 \text{ ms}$  was assumed in the simulation model.

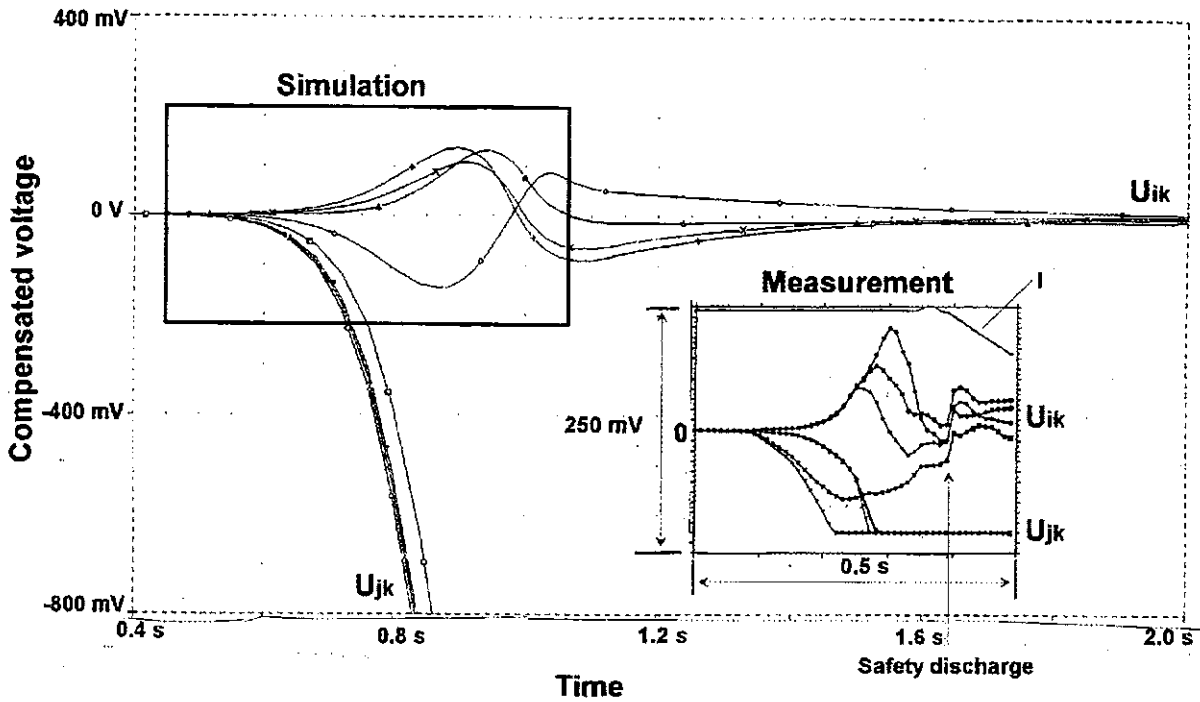


Fig. 27. Compensated voltages during **quench in DP4** after slowly ramping up to a current of 24.2 kA ( $U_{ik} = U(\text{DP3})$ ,  $U_{jk} = U(\text{DP4})$ ). In the simulation was assumed that the lengths of the resistive zones rise exponentially to final values of 1.1 mΩ at  $t \approx 930$  ms (time of safety discharge) and stay constant thereafter. In the simulation **the starting point for the quench process differs up to 30 ms from subcable to subcable**

Considering the long time constants involved with current sharing the statement that quench occurred in all subcables at about the same time can be made. That statement is confirmed by the measured compensated voltage patterns shown in Fig. 28 and 29. Performing numerous simulations, as the one shown in Fig. 30, leads to only one possible explanation for these compensated voltage patterns:

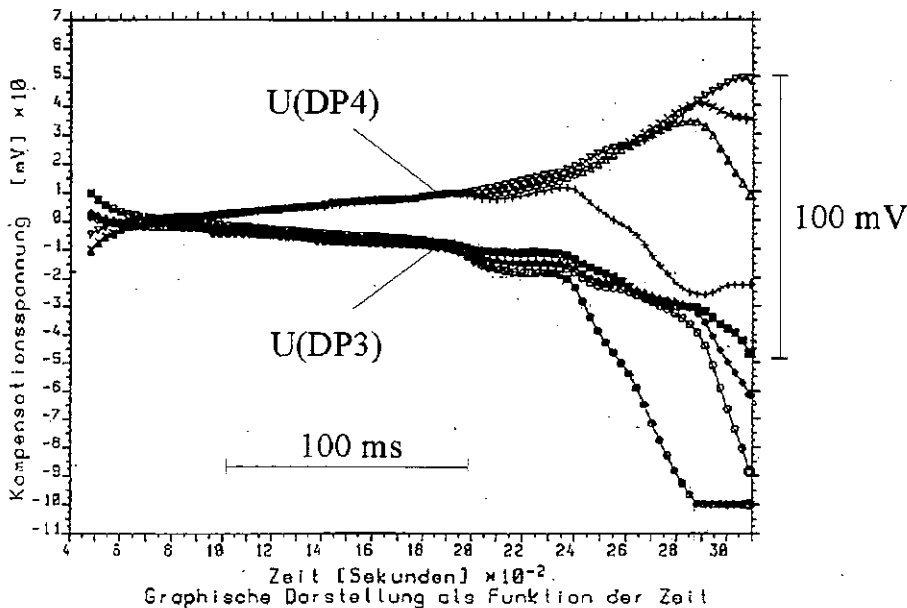


Fig. 28. Measured compensated voltages during **quench in DP3** following a half-coil discharge (current level: 27.25 kA in DP3 and DP4, no current in DP1 and DP2)

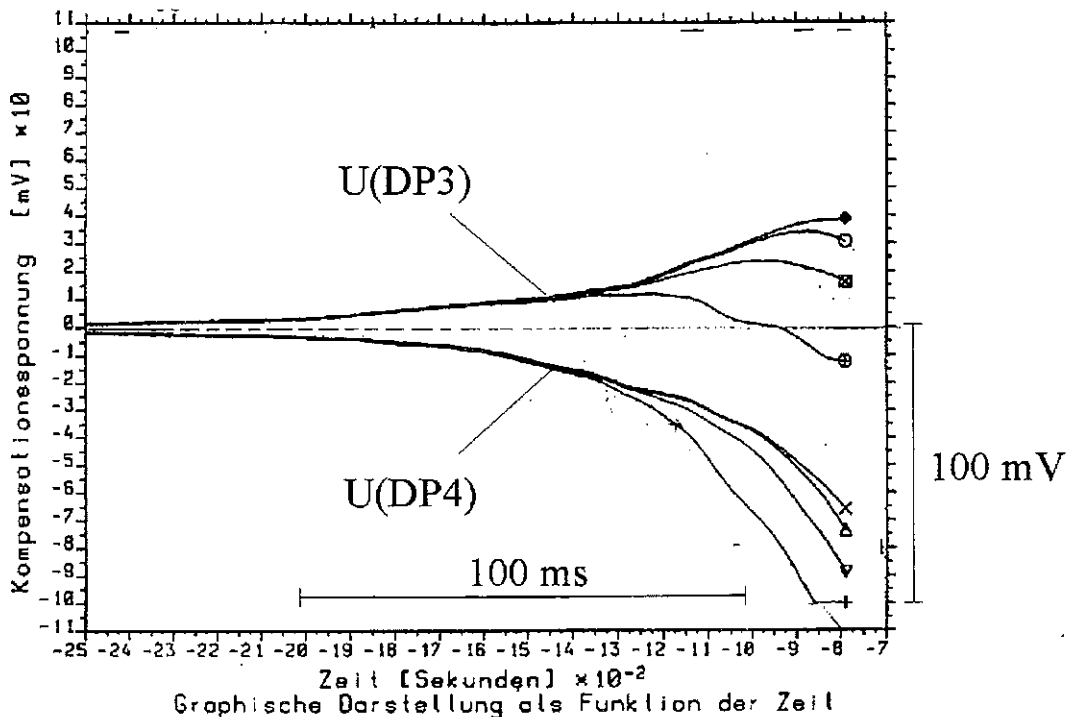


Fig. 29. Measured compensated voltages during **quench in DP4** after slowly ramping up (coil current: 24.7 kA)

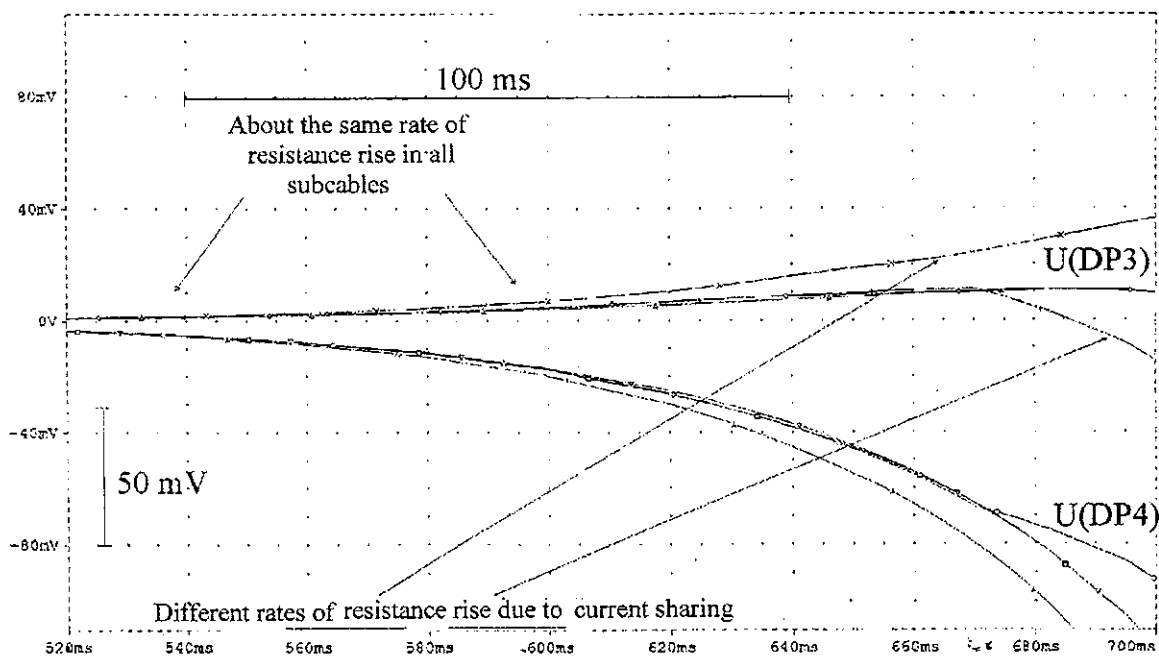


Fig. 30. Calculated compensated voltages during **quench in DP4** (coil current: 25 kA). **In the simulation was assumed that the quench process starts in all subcables at the same time** and that the growth rate of the resistive zones is the same in all subcables until  $t \approx 620$  ms. Thereafter the resistance rise rate was slightly varied from subcable to subcable.

Such compensated voltage patterns ("trumpets") are only possible if quenches occur in all subcables at the same time and with about the same rate of propagation. The oc-

currence of such "trumpets" substantiates the statement that the POLO cable had an extremely homogeneous current distribution directly after ramping which can only be achieved by a very low rate of irregularities in the geometry of the subcables, cables, and winding. The statement that the current distribution was homogeneous in the POLO cable is confirmed by the fact that the POLO coil reached the stability limit expected from measured cable parameters and showed no unexpected RRL phenomena [27].

The circumstance that some of the purely inductive compensated voltages in DP 3 have the same orientation as the partly resistive voltages in DP 4 can be explained by current sharing (see Fig. 30).

The subcable currents belonging to the compensated voltages in Fig. 27 and 30 are shown in Fig. 31 and 32. Fig. 31 can give a realistic impression on the order of magnitude of subcable currents being exchanged across the current leads during the first 200 ms after quench initiation.

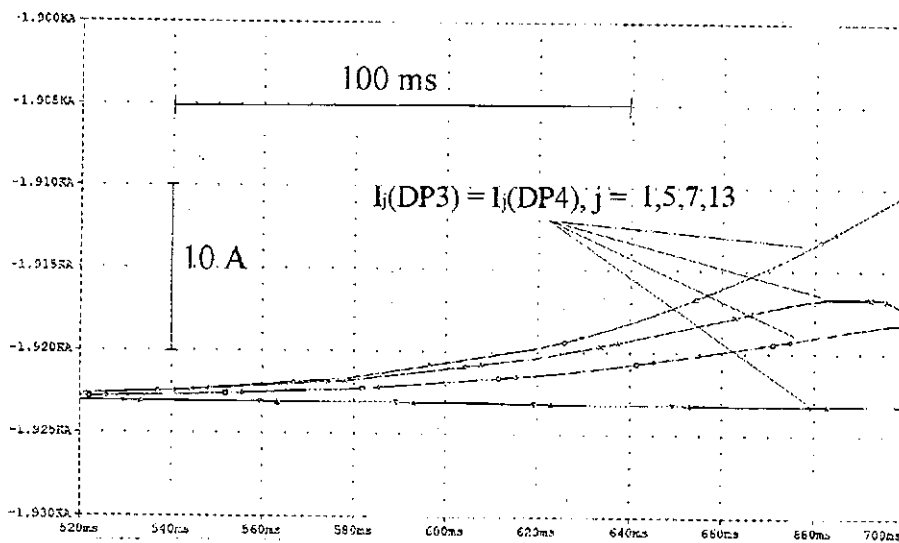


Fig. 31. Calculated subcable currents during **quench in DP4**. The currents belong to the compensated voltages in Fig. 30 (same simulation and same time window as in Fig. 30)

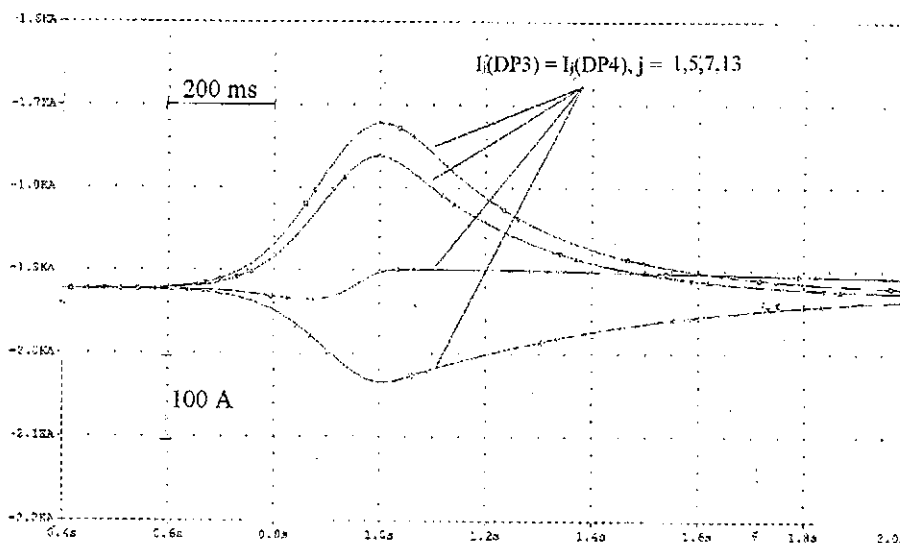


Fig. 32. Calculated subcable currents during **quench in DP4** after slowly ramping up. The currents belong to the compensated voltages in Fig. 27 (same simulation and same time window as in Fig. 27)

The size of the subcable currents shown in Fig. 32 is only realistic for  $t < 930$  ms. Thereafter the safety discharge of the POLO coil was initiated leading to different subcable currents than the ones shown here. In Fig. 32 the subcable currents converge for  $t \rightarrow \infty$  because it was assumed in the simulations that the resistive zones stay constant after reaching maximum values of  $1.1 \text{ m}\Omega/\text{s}$ .

## B. Quench in the CuNi half of the POLO coil

Since the analysis of current sharing in non-insulated strands is very complicated even for simplified cable models [9, 15-16] or cables of short lengths [14, 17], the analysis of current redistribution after quench in a real-size magnet was concentrated on that half of the POLO coil where the subcables are insulated from each other by Glass-Kapton-Glass (GKG) strips. The electro-dynamics of current sharing processes in the CuNi half of the POLO coil are very complex since the quench zones cause locus dependent currents flowing between the subcables, and initially current sharing occurs in small regions only. **Therefore the simulation model used in section III can only be used for calculating the overall behaviour of the CuNi half of the POLO coil during quench.** A detailed investigation of the current sharing process in cables with non-insulated strands requires a more detailed model.

In order to substantiate a statement made in chapter III, saying that the network model shown in Fig. 18 can be used for simulating the effects of disturbances in the inductance matrix of magnets being wound from cables with non-insulated strands, simulations were performed with that model using transverse resistances  $R_{\text{trans}} = 180 \text{ n}\Omega$ . These values correspond to the transverse resistance between two subcables along four turns of the POLO coil and are one order of magnitude higher than the ones used in chapter III. Simulating a quench in all subcables under these conditions, an immediate current transfer across these transverse resistances occurs (see Fig. 33 and 34).

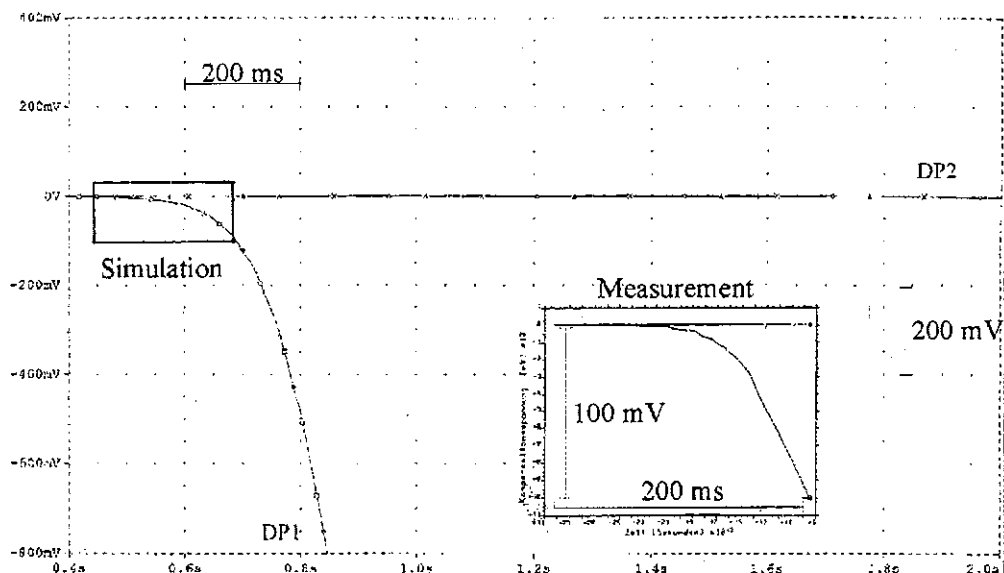


Fig. 33. **Measured compensated voltage at quench in DP1 and corresponding simulated overall behaviour.** In the simulation was assumed that the lengths of the resistive zones rise exponentially to final values of  $1.1 \text{ m}\Omega$  at  $t \approx 930$  ms (time of safety discharge) and stay constant thereafter. In the simulation **the starting point for the quench process differs up to 30 ms from subcable to subcable**

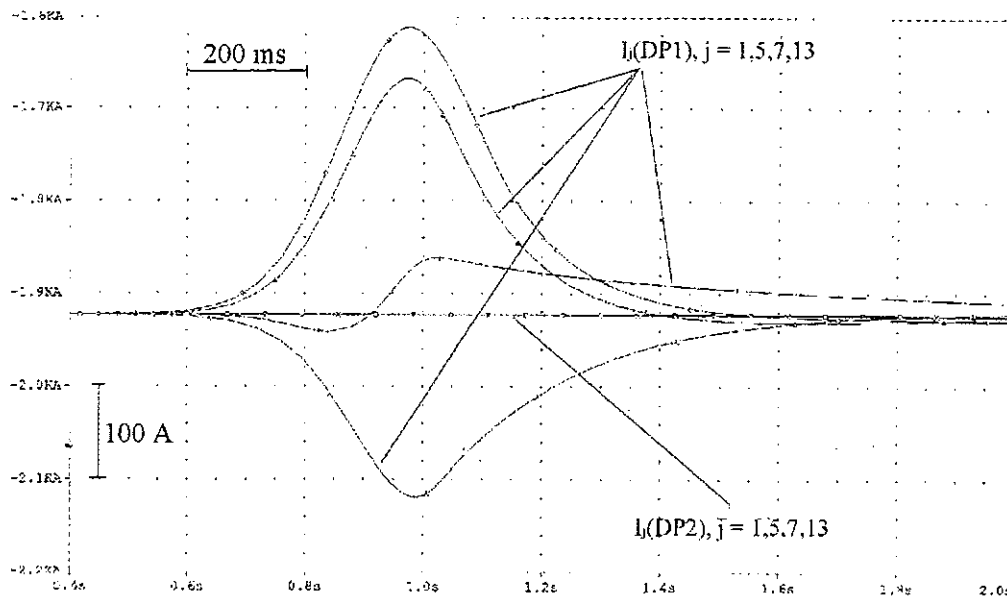


Fig. 34. Calculated subcable currents belonging to the compensated voltages shown in Fig. 33

The same quench propagation model as in section IV.A.2 was used in the simulation. In the simulation result shown in Fig. 33 only one curve for the compensated voltage in DP 1 and DP 2 is visible. Actually all traces are displayed but they lay one on top of the other.

The simulation shows that in case of a quench current sharing occurs across the transverse resistances due to the relative high voltages involved with the resistive zones. **Although the transverse conductivity was modelled in a simple way (see Fig. 18), the calculated compensated voltages agree well with the measured ones.**

Although in chapter III values for  $R_{trans}$  were used being one order of magnitude lower than the ones used here, intercable currents could only be effective at the beginning of the current redistribution processes described on page 30, thus not having a remarkable influence on the electrodynamics of subcable current distribution. **Therefore the network model in Fig. 18 could be used for the calculations presented in chapter III where the electrodynamics of subcable current distribution in cables with non-insulated subcables were investigated during and after ramping. Beyond that, it seems from the good agreement of the calculated and measured compensated voltages in Fig. 33 that such a network model can also be used for calculating the basic parameters of the process of current redistribution in cables with non-insulated subcables during quench.**



## V. Conclusion

A detailed electromagnetic model of the POLO conductor was developed. It considers all magnetic couplings between the subcables and was used to model one half of the POLO coil. The good agreement of the calculated and measured subcable voltages during quench of the POLO coil shows that the model is not only suited for a qualitative simulation of the electro-dynamics of current distribution in conductors with non-insulated subcables, but also for a quantitative simulation of the electro-dynamics of current distribution in conductors with insulated subcables.

Simulations with that model show that subcable connections with varying contact resistances (variance  $\leq 50\%$ ) can not be responsible for Ramp Rate Limitation (RRL) phenomena in superconducting magnets with parameters comparable to those of the POLO coil.

Minor irregularities in the geometry of the conductors and winding of a magnet can not be prevented during the fabrication process. With respect to the unbalances in the cable inductance matrix which can be caused by such defects, it was shown that the POLO conductor concept is less critical for AC applications than, e.g., the Cable-in-Conduit-Conductor (CICC) concept. Referring to this, the process of compacting the transposed conductor is a very critical issue.

Simulations performed with the POLO half coil model showed that minor unbalances in the cable inductance matrix of a magnet can cause major inhomogeneities of the current distribution in the conductor cross section, due to the ILL effect (ILL = Intensification by Lenz's Law).

In cable experiments with short lengths the electro-dynamics of subcable current distribution differ by orders of magnitude from the electro-dynamics of subcable current distribution in a magnet. Even major disturbances in the symmetrical structure of the cable can therefore only become visible in short length cable experiments if high ramp rates are used.

It was demonstrated that minor irregularities in the geometry of the conductors and winding can also explain the existence and time dependence of large supercurrents in magnets being wound from cables with insulated and non-insulated strands. The supercurrents may explain the RRL phenomena observed in fusion magnets [4, 9]. Only high transverse conductivities between subcables have a positive influence on the homogeneity of current distribution after ramping. But in magnets being wound from conductors with sufficient transverse conductivity the ramp rate would be limited due to coupling losses.

The pattern of the compensated voltages in quenching the magnet were analysed during the POLO experiment by comparison of simulation and measurement. It was shown that the cable symmetry is the most important reason for having a homogeneous current distribution after ramping and that the POLO conductor has fulfilled that symmetry requirement. From these results it can be concluded that a very low rate of irregularities in the geometry of the cables and winding is the most important prerequisite for a good AC performance of a magnet.

## ACKNOWLEDGEMENT

The fruitful discussions with C. Schmidt and the efforts of all colleagues involved with the POLO experiment are gratefully acknowledged.

---

## REFERENCES

- [1 ] Krempasky L., Schmidt C, "Influence of a longitudinal variation of dB/dt on the magnetic field distribution of superconducting accelerator magnets", © 1995 American Institute of Physics, pp. 1545 - 1547
- [2 ] Gosh A. K., Robins K. E., Sampson W. B., Proceedings of the 1993 Particle Accelerator Conference, Washington, DC, 1993 (in press)
- [3 ] H. Brück, et al., DESY report HERA 91-01, Hamburg, Germany, 1991 (unpublished)
- [4 ] L. Krempasky, C. Schmidt, "A Possible Explanation of the Problem of Ramp Rate Limitation in Large Superconducting Magnets", 14th Int. Conf. on Magnet Technology, paper B 41, Tampere, Finland, June 1995 (to be published)
- [5 ] Painter T. A., et al., "Test Data from the US-Demonstration Poloidal Coil Experiment", MIT Plasma Fusion Center, Cambridge 1992, MA
- [6 ] Takayasu M., et al., "Measurements of Ramp-Rate Limitation of Cable-in-Conduit Conductors", IEEE Trans. on Applied Superconductivity, Vol. 3 (1993), pp. 456-459
- [7 ] Vysotsky V., et al., "New Methode of Current Distribution Studies for Ramp Rate Stability of Multistrand Superconducting Cables", Applied Superconductivity Conference, Boston, MA, 1994 (to be published)
- [8 ] Ferri M. A., "Memorandum: Current Distribution and Ramp Rate Limitation in CICC's", ITER/US/94/EV-MAG/M.FERRI/10.11/1, October 11, 1994 (unpublished)
- [9 ] L. Krempasky, C. Schmidt, "Theory of 'supercurrents' and their influence on field quality and stability of superconducting magnets", to be published in Journal of Applied Physics, November 1995
- [10 ] M. Darweschad, A. Ulbricht et al., "The POLO coil, a prototype tokamak poloidal field coil, design features and test results", 14th Int. Conf. on Magnet Technology, paper B12, Tampere, Finland, June 1995 (to be published)
- [11 ] Förster S., Jeske U., Nyilas A., "Fabrication of a 15 kA NbTi-cable for the 150 T/s high ramp rate POLO Model Coil", Fusion Technology 1988, © Elsevier Science Publishers B. V., 1989, Vol.2, pp. 1557-1564
- [12 ] Gosh A. K., Robins K. E., Sampson W. B., Int. J. Mod. Phys. A, Suppl. 2B, 665 (1993)

- 
- [13] Tsuda M., Shimada T., Takada Y., Okazaki K., Ishiyama A., "Current Distribution in A.C. Multi-strand Superconducting Cables", Dept. of Electrical Engineering, Waseda Univ., 3-4-1 Ohkubo, Shinjuku-ku, Tokyo 169, Japan, Cryogenics 1994, Vol 34, ICEC Supplement pp. 555 - 558
- [14] K. Mori, Y. Suzuki, N. Hara, M. Kitamura, T. Tominaka, "Current Distribution Characteristics of Superconducting Parallel Circuits", IEEE Transactions on Magnetics, Vol. 30, NO. 4, July 1994, pp. 1919-1922
- [15] Turck B., "Influence of a transverse conductance on current sharing in a two-layer superconducting cable", Cryogenics, August 1974, pp. 448 - 454
- [16] Ries G., "Stability in superconducting multistrand cables", Cryogenics, September 1980, pp. 513 - 519
- [17] Tsuda M., Okazaki K., Hashizume H., Ishiyama A., "Influence of Current Distribution on Quench Process in Non-insulated AC Multi-strand Superconducting Cables", Applied Superconductivity Conference paper LLA-11, Boston, MA, 1994 (to be published)
- [18] S. J. Sackett, "EFFI - A Code for Calculating the Electromagnetic Field, Force, and Inductance in Coil Systems of Arbitrary Geometry", UCRL-52402, 1978
- [19] C. Kill, W. Maurer, "HELIX - An Input Generator for EFFI", KfK 5191, Mai 1993
- [20] F. W. Grover, "Inductance Calculations", Dover Publications Inc., New York, 1946
- [21] A. M. Miri, C. Sihler, M. Irmisch, A. Ulbricht, "Transient Voltage Oscillations in a Large Superconductive Coil", Proc. of the 9th Int. Symp. on High Voltage Engineering, Graz, Austria, August 1995, pp. 6744-1 - 6744-4
- [22] MicroSim Corporation, "The Design Center" Version 5.4, Irvine, California 92718, July 1993
- [23] G. Friesinger, U. Jeske, A. Ulbricht et al., "Specific Fabrication Techniques of the POLO Model Coil and its Components", IEEE Transactions on Magnetics, Vol. 28, No. 1, January 1992, pp. 271-274
- [24] W. Maurer, R. Heller, M. Irmisch, unpublished KfK report, Karlsruhe, July 1993
- [25] H. Bayer, A. Ulbricht et al., "Test of the POLO model coil - a superconducting poloidal field coil according to the specifications of the tokamak operation - in the KfK TOSKA facility, Proc. of the 18th SOFT, Karlsruhe, August 1994, pp. 917-920
- [26] H. Tateishi, C. Schmidt, "Experimental Study of Stability Against Magnetic Pulse Fields of the KfK Poloidal Field Coil Cable", Cryogenics 1993 Vol. 33, No 6, pp. 615-628
- [27] R. Heller, C. Schmidt, A. Ulbricht, F. Wüchner, "Stability of a Poloidal Field Coil in Rapidly Changing Magnetic Fields", 14th Int. Conf. on Magnet Technology, paper B 40, Tampere, Finland, June 1995 (to be published)

